EXACT RIEMANN SOLUTIONS TO SHALLOW WATER EQUATIONS

By

EE HAN (*Institut fuer Analysis und Numerik, Otto-von-Guericke-Universitaet Magdeburg, D-39106 Magdeburg, Germany*)

AND

GERALD WARNECKE (*Institut fuer Analysis und Numerik, Otto-von-Guericke-Universitaet Magdeburg, D-39106 Magdeburg, Germany*)

Abstract. We determine completely the Riemann solutions to the shallow water equations with a bottom step, including the dry bed problem. The nonstrict hyperbolicity of this first-order system of partial differential equations leads to resonant waves and nonunique solutions. To address these difficulties we construct the L–M and R–M curves in the state space. For the bottom step elevated from left to right, we classify the L–M curve into five different cases and the R–M curve into two different cases based on the subcritical and supercritical Froude number of the Riemann initial data as well as the jump of the bottom step. The behaviors of all basic cases of the L–M and R–M curves are fully analyzed. We observe that the non–uniqueness of the Riemann solutions is due to bifurcations on the L–M or R–M curves. The possible solutions including classical waves and resonant waves as well as dry bed state are solved in a uniform framework for any given Riemann initial data.

1. Introduction. In this paper we are concerned with the shallow water system of hyperbolic equations, which can be written in the form

$$\frac{\partial \mathbf{W}}{\partial t} + \frac{\partial \mathbf{F}(\mathbf{W})}{\partial x} = -\mathbf{H}(\mathbf{W})z_x, \qquad (1.1)$$

where

$$\mathbf{W} = \begin{bmatrix} z \\ h \\ hu \end{bmatrix}, \quad \mathbf{F}(\mathbf{W}) = \begin{bmatrix} 0 \\ hu \\ hu^2 + gh^2/2 \end{bmatrix}, \quad \mathbf{H}(\mathbf{W}) = \begin{bmatrix} 0 \\ 0 \\ gh \end{bmatrix}; \qquad (1.2)$$

see, e.g., Stoker [2]. The independent variables z, h and u denote, respectively, the bottom topography, the water height and the water velocity, while g is the gravity constant. Usually the bottom topography z is assumed to be given a priori.

The shallow water equations (1.1) model incompressible flows on a bottom bed under the assumption that the depth of the fluid is much smaller than the wave length of the disturbances considered. It has wide applications in fluid dynamics; for example, tidal flows in an estuary, hydraulic jumps, river beds and channels, tsunamis, etc. The system has also been studied from a mathematical point of view. A particular feature of the system (1.1) is the presence of the bottom topography $z(x)$. This geometric variable is independent of time and leads to a stationary source and a nonconservative term.

We only reference a few publications. LeFloch [18] complemented a related nonconservative system with an additional trivial equation $z_t = 0$. It introduces a linear degenerate field with a 0–speed eigenvalue. As a result the system (1.1) becomes a nonstrictly hyperbolic system. Due to the coincidence of eigenvectors the system becomes degenerate at sonic states; see, e.g., Alcrudo and Benkhaldoun [5]. Bernettia et al. [7] studied an enlarged system and used the energy to rule out solutions that are physically inadmissible. Andrianov [3] proposed an example which has two solutions for one set of initial data to show that different numerical schemes may approach different exact solutions. Li and Chen [10] studied the generalized Riemann problem for the current system. LeFloch and Thanh in [19, 20] investigated the exact Riemann solutions. They obtained most of the possible solutions for given initial data. However, they omitted one possible type of solution, which is denoted as the wave configuration E in this work. Moreover, they did not give complete proofs for the existence and uniqueness of the solutions, especially for the conjecture in [20, Remark 6, p. 7646]. Besides the papers we just mentioned, considerable work has been devoted to the topic of the shallow water equations; see, e.g., [1, 2, 12, 14] and the references therein.

In this work we propose a uniform framework to solve the system (1.1) with the following Riemann initial data

$$\mathbf{W}(x,0) = \begin{cases} \mathbf{W}_L, & x < x_0, \\ \mathbf{W}_R, & x > x_0, \end{cases} \tag{1.3}$$

where $\mathbf{W}_q$ with $q = L$ or R are constant. There are three wave curves for the system (1.1). The first and second wave curves are given by the physically relevant parts of the rarefaction and shock curves. The third wave curve, denoted as the stationary wave curve, is due to the variation of the bottom step. Since the governing system is nonstrictly hyperbolic, the mutual positions of the stationary wave curve with respect to the rest of the two elementary waves cannot be determined a priori. To address this difficulty, we introduce the L–M and R–M curves in the state plane for the construction of solutions to Riemann problems. The idea is motivated by Marchesin and Paes-Leme [21] as well as our previous work for the exact Riemann solutions to Euler equations in ducts with discontinuous cross–section in [9].

During this work we always assume without loss of generality that $z_L < z_R$. The opposite case can be treated as the mirror–image problem by reflecting the Riemann initial data in terms of $x = x_0$ and setting the velocities in the opposite direction. We

take into account the stationary wave curves by deriving a *velocity* function. Owing to this function, the L–M and R–M curves with $z_L < z_R$ can be, respectively, classified into five and two different cases by the subcritical or supercritical Froude number of the Riemann initial data as well as the jump of the bottom step. This new classification is very helpful for a systematic consideration of solutions. It is given for the L–M curves at the beginning of Section 4.2 and for the R–M curves in Section 4.3. Note that each of these curves leads to more than one wave configuration, depending on the Riemann initial data. We obtain the 7 wave configurations, denoted as A, B, C, D, E, F, G, that do not have a dry bed state and 6 that do have a dry bed state in the solution. The dry bed states are like vacuum states in gas dynamics and therefore we index the corresponding wave configurations with subscript letter v.

We find that the water can always spread across a lowered bottom step. But the water can go across an elevated bottom step if and only if a critical step size z_{max} is larger than the actual jump height of the bottom step. The critical step size z_{max} is determined by the height and Froude number of the inflow state.

We carefully study the monotonicity and smoothness properties of the L–M and R–M curves in each case. Note that the introduction of these curves and the use of the velocity function make our approach to the solution of the Riemann problem different from the previous work. We feel that this makes the solution procedure clearer and simpler. Observe that a bifurcation occurs for certain cases. This bifurcation introduces nonunique solutions and validates the conjecture in [20, Remark 6, p. 7646]. Specifically, we solve the dry bed problem of the solution in this framework. Here the dry bed problem refers two subcases. One is for the water propagating to a dry bed; see Toro [11]. The other one is for the dry bed state emerging due to the motion of the flow.

The organization of the paper is as follows. We briefly review the fundamental concepts and notions for the governing system in Section 2. In Section 3 we discuss the stationary wave curves. Our main focus is in Section 4, which contains the definition of the L–M and R–M curves and the complete analysis of their structures. All the possible wave configurations are illustrated in this section. The algorithm for determining the exact solutions is explained in Section 5. Finally we make some conclusions in Section 6.

2. The shallow water system. We now derive the quasilinear form of the system (1.1). Set $\mathbf{V} = (z,\ h,\ u)^T$; then

$$\mathbf{V}_t + \mathbf{A}(\mathbf{V})\mathbf{V}_x = 0, \tag{2.1}$$

where the *Jacobian matrix* $\mathbf{A}(\mathbf{V})$ is in the form

$$\mathbf{A}(\mathbf{V}) = \begin{pmatrix} 0 & 0 & 0 \\ 0 & u & h \\ g & g & u \end{pmatrix}.$$

The eigenvalues of $\mathbf{A}(\mathbf{V})$ are

$$\lambda_0 = 0, \quad \lambda_1 = u - c, \quad \lambda_2 = u + c, \tag{2.2}$$

where $c = \sqrt{gh}$ is the sound speed. The eigenvalues are referred to as the characteristic speeds. The system (1.1) is not strictly hyperbolic as a result of the fact that λ_0 can

coincide with any of the two other eigenvalues. The corresponding right eigenvectors are

$$\mathbf{R}_0 = \begin{pmatrix} \frac{c^2-u^2}{c^2} \\ 1 \\ -\frac{u}{h} \end{pmatrix}, \qquad \mathbf{R}_1 = \begin{pmatrix} 0 \\ 1 \\ -\frac{c}{h} \end{pmatrix}, \qquad \mathbf{R}_3 = \begin{pmatrix} 0 \\ 1 \\ \frac{c}{h} \end{pmatrix}. \qquad (2.3)$$

One can easily show that

$$\mathbf{R}_0 \to \mathbf{R}_k \quad \text{as} \quad \lambda_k \to 0 \quad \text{for} \quad k = 1, 2. \qquad (2.4)$$

Consequently the system (1.1) is degenerate for the states at which the eigenvalues λ_1 or λ_2 coincide with λ_0. Specifically, this state is the sonic state at which $u = \pm c$.

We use the terminology k-waves, $k = 0, 1, 2$, to denote the waves associated to the k–characteristic fields when the eigenvalues are distinct from each other. Here the 1– and 2–waves are shocks (hydraulic jumps) or rarefactions. Traditionally the 0–wave is named the stationary wave due to the jump of the bottom step. Note that a 0–speed shock or a transonic rarefaction wave will coincide with the stationary wave. In such a case these elementary waves will be involved in the stationary wave [15]. We name these combined waves as the resonant waves. They will be studied in detail later; see also Han et al. [9].

We define the shock and rarefaction curves. Let $\mathbf{U}_q = (h_q, u_q)^T$ be any state in the state space. The shock speed σ_k and the velocity u can be expressed as follows:

$$\sigma_k(h; \mathbf{U}_q) = u_q \pm h\sqrt{\frac{g}{2}\left(\frac{1}{h} + \frac{1}{h_q}\right)}, \qquad (2.5)$$

$$u = u_q \pm (h - h_q)\sqrt{\frac{g}{2}\left(\frac{1}{h} + \frac{1}{h_q}\right)}, \qquad (2.6)$$

where $h > h_q$ and the subscript $k = 1, 2$ represents the number of the wave family. The sign $-$ is taken when $k = 1$ while the sign $+$ is taken when $k = 2$. The detailed derivation can be found in Francisco and Benkhaldoun [5]. The admissible shock curves $S_k(\mathbf{U}_q)$, $k = 1, 2$ denote the states which are connected to the state $\mathbf{U}_q$ by an admissible 1–shock or 2–shock respectively. Set

$$S_k(\mathbf{U}_q) = \left\{(h, u) \mid u = u_q \pm (h - h_q)\sqrt{\frac{g}{2}\left(\frac{1}{h} + \frac{1}{h_q}\right)} \text{ with } h > h_q\right\}, \ k = 1, 2. \qquad (2.7)$$

Generally the shock curve $S_k(\mathbf{U}_q)$ contains three components, namely,

$$\begin{aligned} S_k^{\pm}(\mathbf{U}_q) &= \left\{(h, u) \mid (h, u) \in S_k(\mathbf{U}_q) \text{ and } \sigma_k(h; \mathbf{U}_q) \gtrless 0\right\}, \\ S_k^0(\mathbf{U}_q) &= \left\{(h, u) \mid (h, u) \in S_k(\mathbf{U}_q) \text{ and } \sigma_k(h; \mathbf{U}_q) = 0\right\}. \end{aligned} \qquad (2.8)$$

We study the state set $S_k^0(\mathbf{U}_q)$. Note that we have the shock speed

$$\sigma_k(h; \mathbf{U}_q) = u_q \pm h\sqrt{\frac{g}{2}\left(\frac{1}{h} + \frac{1}{h_q}\right)} = 0 \quad \text{with} \quad h > h_q. \qquad (2.9)$$

Therefore, introducing the Froude number $F_q := \frac{u_q}{c_q} = \frac{u_q}{\sqrt{gh_q}}$, we obtain

$$\left(\frac{h}{h_q}\right)^2 + \frac{h}{h_q} - 2F_q^2 = 0. \tag{2.10}$$

There are two solutions to (2.10) which are

$$h_1 = \frac{-1+\sqrt{1+8F_q^2}}{2}h_q, \quad h_2 = \frac{-1-\sqrt{1+8F_q^2}}{2}h_q. \tag{2.11}$$

Note that $h_1 > h_q$ and $h_2 < 0 < h_q$, so h_1 is the physically relevant solution to (2.9). Hence the set $S_k^0(\mathbf{U}_q)$ contains only one state. Hereafter we use $\hat{\mathbf{U}}_q = S_k^0(\mathbf{U}_q)$ to denote it; then we have

$$\hat{h}_q = \frac{-1+\sqrt{1+8F_q^2}}{2}h_q. \tag{2.12}$$

Since $\hat{h}_q \hat{u}_q = h_q u_q$, we get $\hat{u}_q = \frac{h_q u_q}{\hat{h}_q}$. Direct calculation yields

$$\hat{u}_q = \frac{1+\sqrt{1+8F_q^2}}{4F_q^2}u_q. \tag{2.13}$$

For the rarefaction curves, similarly, we use $R_k(\mathbf{U}_q)$ to denote the states $\mathbf{U}$ which can be connected to $\mathbf{U}_q$ by a k–rarefaction wave, i. e.

$$R_k(\mathbf{U}_q) = \{(h, u) \mid u = u_q \pm 2(c - c_q) \text{ with } h \le h_q\}, \quad k = 1, 2. \tag{2.14}$$

2.1. *The* 1–*wave and* 2–*wave curves.* Generally the k–wave curves $T_k(\mathbf{U}_q)$, $k = 1, 2$, are defined as the sets of states which can be connected to the initial state $\mathbf{U}_q$ by admissible waves. That is to say we have

$$T_1(\mathbf{U}_L) = R_1(\mathbf{U}_L) \cup S_1(\mathbf{U}_L), \quad T_2(\mathbf{U}_R) = R_2(\mathbf{U}_R) \cup S_2(\mathbf{U}_R). \tag{2.15}$$

Obviously $T_1(\mathbf{U}_L)$ and $T_2(\mathbf{U}_R)$ are the admissible wave curves associated to the characteristic field with λ_1 and λ_2 in the state space respectively.

For simplicity we define the following function

$$f(h; h_q) := \begin{cases} 2(\sqrt{gh} - c_q), & \text{if } h \le h_q, \\ (h - h_q)\sqrt{\frac{g}{2}\left(\frac{1}{h} + \frac{1}{h_q}\right)}, & \text{if } h > h_q. \end{cases} \tag{2.16}$$

We will consider $f(h; h_q)$ as a function of h for given parameter h_q. Therefore the k–wave curve $T_k(\mathbf{U}_q)$, $k = 1, 2$ can be rewritten as

$$\begin{aligned} T_1(\mathbf{U}_q) &= \{\mathbf{U}|u = u_q - f(h; h_q), \ h \ge 0\}, \\ T_2(\mathbf{U}_q) &= \{\mathbf{U}|u = u_q + f(h; h_q), \ h \ge 0\}. \end{aligned} \tag{2.17}$$

LEMMA 2.1. *The function $f(h; h_q)$ is continuously differentiable, strictly increasing and concave.*

Proof. The function $f(h; h_q)$ is twice continuous due to $\lim\limits_{h \to h_q-} f(h; h_q) = \lim\limits_{h \to h_q+} f(h; h_q) = 0$. The derivative of the function $f(h; \mathbf{Q}_q)$ is

$$f'(h; h_q) := \begin{cases} \sqrt{\frac{g}{h}}, & \text{if } h \le h_q, \\ \sqrt{\frac{g}{2}}\frac{\frac{1}{h} + \frac{2}{h_q} + \frac{h_q}{h^2}}{2\sqrt{\frac{1}{h} + \frac{1}{h_q}}} & \text{if } h > h_q. \end{cases} \tag{2.18}$$

Therefore we have

$$f'(h; h_q) > 0 \qquad (2.19)$$

and $\lim_{h \to h_q} f'(h; h_q) = \sqrt{\frac{g}{h_q}}$. To see the convexity of the function, we need to consider the second derivative of the function $f(h; h_q)$. Actually we have

$$f''(h; h_q) := \begin{cases} -\frac{1}{2}\sqrt{g}h^{-\frac{3}{2}}, & \text{if } h \leq h_q, \\ -\frac{\sqrt{g}}{4\sqrt{2}} \frac{\frac{5}{h^3} + \frac{3h_q}{h^4}}{\left(\frac{1}{h} + \frac{1}{h_q}\right)^{\frac{3}{2}}}, & \text{if } h > h_q. \end{cases} \qquad (2.20)$$

It follows that $f''(h; h_q) < 0$. Moreover, we have $\lim_{h \to h_q} f''(h; h_q) = -\frac{1}{2}\sqrt{g}h_q^{-\frac{3}{2}}$. This is enough to confirm the lemma. $\qquad\square$

Lemma 2.1 reveals that the 1–wave curve $T_1(\mathbf{U}_L)$ is a strictly decreasing concave curve, while the 2–wave curve $T_2(\mathbf{U}_R)$ is a strictly increasing convex curve in the (u, h) state plane. Therefore these two curves have at most one intersection point. To find whether the intersection point exists, we need to consider the state with $h = 0$, which corresponds to the dry bed of the water; see Toro [11]. For the 1–wave curve $T_1(\mathbf{U}_L)$ and the 2–wave curve $T_2(\mathbf{U}_R)$ we take $h = 0$ in (2.17) and (2.16). We obtain two velocities

$$u_{0L} = u_L + 2c_L \qquad (2.21)$$

and

$$u_{0R} = u_R - 2c_R. \qquad (2.22)$$

These are the velocities of the water covering or uncovering a dry state $h = 0$. The two curves $T_1(\mathbf{U}_L)$ and $T_2(\mathbf{U}_R)$ will interact if $u_{0L} \geq u_{0R}$, i.e.

$$u_R - u_L \leq 2(c_L + c_R). \qquad (2.23)$$

In this case the intersection point of $T_1(\mathbf{U}_L)$ and $T_2(\mathbf{U}_R)$ uniquely exists. Otherwise, if $u_{0L} < u_{0R}$, there is no intersection point. The solution involves a dry bed intermediate state.

Next we turn to study two specific dry bed problems. Both of them concern the water receding from the jump of the dry bed. The first problem has the Riemann initial data

$$(h, u)(x, 0) = \begin{cases} (h_L, u_L), & x < 0, \\ (0, 0), & x > 0, \end{cases} \qquad (2.24)$$

with the restriction that $u_{0L} < 0$. In such a case the 2–wave of the solution is missing while the 1–wave is a rarefaction wave on the left side. The corresponding solution is given as

$$(h, u)(x, t) = \begin{cases} (h_L, u_L), & \frac{x}{t} \leq u_L - c_L, \\ \left(\frac{\left(u_L + 2c_L - \frac{x}{t}\right)^2}{9g}, \frac{u_L + 2c_L + 2\frac{x}{t}}{3}\right), & u_L - c_L < \frac{x}{t} < u_{0L}, \\ (0, 0), & \frac{x}{t} > u_{0L}. \end{cases} \qquad (2.25)$$

The other problem has the Riemann initial data

$$(h, u)(x, 0) = \begin{cases} (0, 0), & x < 0, \\ (h_R, u_R), & x > 0, \end{cases} \qquad (2.26)$$

with $u_{0R} > 0$. Similarly, the 1–wave of the solution is missing and the 2–wave is a rarefaction wave on the right side. The exact solution of this case is shown in the following:

$$(h, u)(x, t) = \begin{cases} (h_R, u_R), & \frac{x}{t} \geq u_R + c_R, \\ \left(\frac{\left(u_R - 2c_R - \frac{x}{t}\right)^2}{9g}, \frac{u_R - 2c_R + 2\frac{x}{t}}{3} \right), & u_R + c_R > \frac{x}{t} \geq u_{0R}, \\ (0, 0), & \frac{x}{t} < u_{0R}. \end{cases} \qquad (2.27)$$

The jump of the bottom step does not affect the solution in these two examples. However for the Riemann problem (1.1), (2.24) or (2.26) but with $u_{0L} > 0$ or $u_{0R} > 0$ respectively, the jump of the bottom step induces an additional wave. The motion of the flow becomes more complicated, not to mention the general Riemann problem of (1.1) and (1.3) with $h_L > 0$ and $h_R > 0$. There the jump of the bottom step greatly affects the motion of the flow. So, in the next section, we study the stationary wave due to the jump of the bottom step.

3. The stationary wave curve.
The stationary wave curve for the system (1.1) is defined by the ODE system

$$\frac{\partial \mathbf{F}(\mathbf{U})}{\partial x} = -\mathbf{H}(\mathbf{U}) z_x. \qquad (3.1)$$

Motivated by Alcrudo and Benkhaldoun [5] and references cited therein, we have the following Lemma.

LEMMA 3.1. For the smooth bottom topography the sonic state can only appear when the bottom function reaches a maximum.

Proof. The ODE system (3.1) asserts the following equations

$$\begin{aligned} \frac{\partial hu}{\partial x} &= 0, \\ u \frac{\partial u}{\partial x} + g \frac{\partial h + z}{\partial x} &= 0. \end{aligned} \qquad (3.2)$$

Therefore we have

$$\left(1 - \frac{u^2}{c^2}\right) \frac{h}{u} u_x = z_x. \qquad (3.3)$$

The relation (3.3) shows that for smooth lowered bottom topography, i.e. $z_x < 0$, the velocity of the water decreases when $u^2 < c^2$ and vice versa. Similarly for smooth elevated bottom topography, i.e. $z_x > 0$, the velocity increases when $u^2 < c^2$ and vice versa. So we can conclude that the quantity z as a function of x has a maximum at the sonic state $u^2 = c^2$. $\qquad \square$

In this work we regard the stationary wave as a transition layer located at $x = 0$ with 0 width. In this approach the discontinuous variation of the bottom step is viewed as the limiting case of locally monotonic bottom slope going to infinity. This idea has been used by Alcrudo and Benkhaldoun [5], LeFloch and Thanh [19, 20], Toro [11] etc. for the shallow water systems. Han et. al. [9] also adopted it to solve the Riemann problem for duct flows.

3.1. *The stationary wave.* In this section we use the subscript i to signify the inflow variables and o to signify the outflow variables. Assume that the piecewise constant bottom topography has the values z_i and z_o, while the upstream flow state is $(h_i,\ u_i)$ (which is known) and the downstream flow state is (h, u). Here z_i will be z_L if $u > 0$, while it is z_R if $u < 0$. With the analogous consideration z_o will be determined.

Let us assume that $h_i,\ h > 0$. One can easily derive the following relations from the system (3.1)

$$hu \ = \ h_i u_i, \tag{3.4}$$

$$\frac{u^2}{2} + g(h + z_o) \ = \ \frac{u_i^2}{2} + g(h_i + z_i). \tag{3.5}$$

The formula (3.4) implies the following conditions:
(1) u_i and u have the same sign,
(2) $u_i = 0 \iff u = 0$.

Our aim is to calculate the downstream state (h, u). Specifically if $u_i = 0$ and $h_i + z_i - z_o > 0$, we have $u = 0$ and $h = h_i + z_i - z_o$. Otherwise if $u_i = 0$ and $h_i + z_i - z_o < 0$, we have $u = 0$ and $h = 0$. In the following analysis we always assume that $u_i \neq 0$. For simplicity we can use the notation $\mathbf{U} = \mathbf{J}(z_o; \mathbf{U}_i, z_i)$ to represent the explicit solution $\mathbf{U} := (h, u)$ implicitly given by (3.4) and (3.5). Our aim is to calculate the downstream state (h, u) of the flow for the known upstream flow (h_i, u_i). A *velocity* function is derived from (3.4) and (3.5) to be

$$\Psi(u; \mathbf{U}_i, z_i, z_o) := \frac{u^2}{2} + \frac{c_i^2 u_i}{u} - \frac{u_i^2}{2} - g h_i + g(z_o - z_i). \tag{3.6}$$

The behavior of the velocity function is analyzed in the following lemma.

LEMMA 3.2. Consider

$$u^* = \left(u_i c_i^2\right)^{\frac{1}{3}}. \tag{3.7}$$

Then the velocity function $\Psi(u; \mathbf{U}_i, z_i, z_o)$ has the following properties:
(1) $\Psi(u; \mathbf{U}_i, z_i, z_o)$ decreases if $u < u^*$;
(2) $\Psi(u; \mathbf{U}_i, z_i, z_o)$ increases if $u > u^*$;
(3) $\Psi(u; \mathbf{U}_i, z_i, z_o)$ has the minimum value at $u = u^*$. Moreover, we have $(u^*)^2 = (c^*)^2$.

Proof. The velocity function $\Psi(u; \mathbf{U}_i, z_o)$ is smooth since if $u_i > 0$ the existence region for u is $u > 0$,. Otherwise if $u_i < 0$ the existence region for u is $u < 0$. Therefore the derivative of $\Psi(u; \mathbf{U}_i, z_i, z_o)$ is

$$\frac{\partial \Psi(u; \mathbf{U}_i, z_i, z_o)}{\partial u} = u - \frac{u_i c_i^2}{u^2}. \tag{3.8}$$

Consequently we get

$$\frac{\partial \Psi(u; \mathbf{U}_i, z_i, z_o)}{\partial u} \begin{cases} < 0, & \text{if } u < u^*, \\ = 0, & \text{if } u = u^*, \\ > 0, & \text{if } u > u^*. \end{cases} \tag{3.9}$$

It follows that the velocity function $\Psi(u; \mathbf{U}_i, z_i, z_o)$ is decreasing when $u < u^*$, increasing when $u > u^*$ and has the minimum value at $u = u^*$.

Since

$$c^2 = gh \quad = \quad \frac{gh_i u_i}{u}, \tag{3.10}$$

we get the formula

$$u\frac{\partial \Psi}{\partial u}(u; \mathbf{U}_i, z_i, z_o) = u^2 - \frac{gu_- h_-}{u} = u^2 - c^2. \tag{3.11}$$

From $\frac{\partial \Psi(u^*; \mathbf{U}_i, z_i, z_o)}{\partial u} = 0$ we obtain $(u^*)^2 = (c^*)^2$. $\qquad\square$

REMARK 3.3. Lemma 3.2 shows that the equation $\Psi(u; \mathbf{U}_i, z_i, z_o) = 0$ may have two, one or no solutions. Further discussions are as follows.

(1) If the minimum value $\Psi(u^*; \mathbf{U}_i, z_i, z_o) < 0$, the equation $\Psi(u; \mathbf{U}_i, z_i, z_o) = 0$ has two roots. Assume that the root closer to 0 is u_l and the other one is u_r, with c_l and c_r being the corresponding sound speeds. Then according to (3.11), $u_l^2 - c_l^2 < 0$ and $u_r^2 - c_r^2 > 0$. It is well known that the transition from subcritical to supercritical channel flow can only occur at points of maximum of the bottom function [5]. So physically we can take the one which satisfies

$$\mathrm{sign}(u_q^2 - c_q^2) = \mathrm{sign}(u_i^2 - c_i^2) \tag{3.12}$$

where $q = l$ or r. However, one special case is that if the inflow state $\mathbf{U}_i$ is a sonic state, i.e. $u_i^2 = c_i^2$, then (3.12) no longer holds. There are two possible solutions u_l and u_r to the corresponding velocity function (3.6); which one is to be chosen depends on the requirement of the specific problem. The details will be given later.

(2) If $\Psi(u^*; \mathbf{U}_i, z_i, z_o) = 0$, the equation $\Psi(u; \mathbf{U}_i, z_i, z_o) = 0$ has exactly one solution which is the sonic state, i.e. $u = u^*$.

(3) If $\Psi(u^*; \mathbf{U}_i, z_i, z_o) > 0$, the equation $\Psi(u; \mathbf{U}_i, z_i, z_o) = 0$ has no solution.

The procedure for calculating the outflow state $\mathbf{U} = \mathbf{J}(z_o; \mathbf{U}_i, z_i)$ is summarized in Algorithm 1. However it is necessary to analyze the existence region for $\mathbf{U} = \mathbf{J}(z_o; \mathbf{U}_i, z_i)$ to determine it a priori.

3.2. *Existence of the stationary wave.* Remark 3.3 reveals that the velocity function may have no solutions. To be more precise, we now consider the existence conditions for the outflow state (h, u) of the stationary wave introduced above. According to Lemma 3.2, it is equivalent to evaluate the minimum value of the velocity function $\Psi(u; \mathbf{U}_i, z_i, z_o)$ being not larger than 0, i.e.

$$\Psi(u^*; \mathbf{U}_i, z_i, z_o) = \frac{3}{2}\left(u_i c_i^2\right)^{\frac{2}{3}} - c_i^2 - \frac{u_i^2}{2} + g(z_o - z_i) \leq 0. \tag{3.13}$$

We introduce the *Froude number* $F_i := \frac{u_i}{c_i}$; then we have

$$h_i\left(\frac{3}{2}\left(F_i\right)^{\frac{2}{3}} - \frac{F_i^2}{2} - 1\right) + z_o - z_i \leq 0. \tag{3.14}$$

Therefore we obtain

$$z_o - z_i \leq h_i\left(\frac{F_i^2}{2} - \frac{3}{2}F_i^{\frac{2}{3}} + 1\right). \tag{3.15}$$

We know that

$$\frac{F_i^2}{2} - \frac{3}{2}F_i^{\frac{2}{3}} + 1 \geq 0. \tag{3.16}$$

Algorithm 1 Algorithm for solving $\mathbf{U} = \mathbf{J}(z_o; \mathbf{U}_i, z_i)$

Require: $flag$, z_i, z_o and (h_i, u_i)

1: **if** $z_i = z_o$ **then**
2:     **return** (h_i, u_i)
3: **else if** $u_i = 0$ **then**
4:     **if** $h_i + z_i < z_o$ **then**
5:         **return** $(0, 0)$
6:     **else**
7:         **return** $(h_i + z_i - z_o, 0)$
8:     **end if**
9: **else**
10:     $\Psi_{min} \leftarrow \Psi(u^*; \mathbf{U}_i, z_i, z_o)$
11:     **if** $\Psi_{min} < 0$ **then**
12:         Solve $\Psi(u; \mathbf{U}_i, z_i, z_o) = 0$ by the iteration method to obtain u_l and u_r
13:         $c_l^2 \leftarrow g\frac{h_i u_i}{u_l}$, $c_r^2 \leftarrow g\frac{h_i u_i}{u_r}$
14:         **if** $\text{sign}(u_l^2 - c_l^2) = \text{sign}(v_i^2 - c_i^2) \vee \left(flag = 0 \wedge v_i^2 = c_i^2\right)$ **then**
15:           **return** $(\frac{h_i u_i}{u_l}, u_l)$
16:         **else if** $\text{sign}(u_l^2 - c_l^2) = \text{sign}(v_i^2 - c_i^2) \vee \left(flag = 1 \wedge v_i^2 = c_i^2\right)$ **then**
17:           **return** $(\frac{h_i u_i}{u_r}, u_r)$
18:         **end if**
19:     **else if** $\Psi_{min} = 0$ **then**
20:         **return** $(\frac{h_i u_i}{u^*}, u^*)$
21:     **else if** $\Psi_{min} > 0$ **then**
22:         **print** No Solution.
23:     **end if**
24: **end if**

It reaches 0 if and only if $F_i = 1$. Hence, the above computation motivates the following theorem.

THEOREM 3.4. *The existence of the solution to the velocity function.*
(1) *If $z_o < z_i$, $\Psi(u; \mathbf{U}_i, z_i, z_o)$ always has solutions.*
(2) *Otherwise if $z_o > z_i$, $\Psi(u; \mathbf{U}_i, z_i, z_o)$ has a solution if and only if*

$$z_o - z_i \le h_i \left(\frac{F_i^2}{2} - \frac{3}{2}F_i^{\frac{2}{3}} + 1 \right). \tag{3.17}$$

Theorem 3.4 indicates that on one hand the water can always spread across the lowered jump of the bottom step; on the other hand, the water can overflow the elevated jump of the bottom step if and only if the bottom step is not too high. Specifically it should be less than a critical value which is determined by the height and the Froude number of the inflow.

REMARK 3.5. For the fixed inflow state $\mathbf{U}_i$ and two outflow bottom steps $z_o^1 < z_o^2$, if $\mathbf{J}(z_o^2; \mathbf{U}_i, z_i)$ exists, then $\mathbf{J}(z_o^1; \mathbf{U}_i, z_i)$ also exists. Since we regard the discontinuous
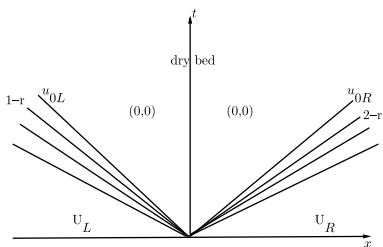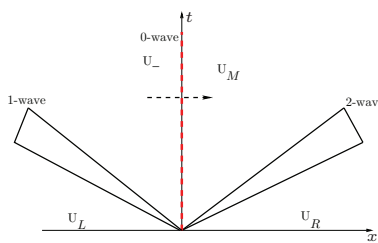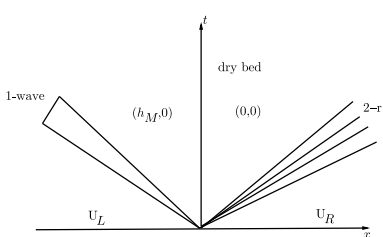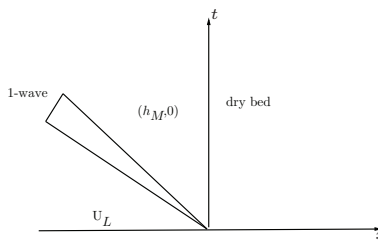
FIG. 1. A_v

FIG. 2. A

FIG. 3. H_1

FIG. 4. H_2

bottom step as the limiting case of monotonic bottom step, it make sense to assume that the solution inside this transition layer is also continuous if there is no resonant wave.

4. L–M and R–M wave curves.

In this work we always assume without loss of generality that

$$z_L < z_R. \tag{4.1}$$

According to Lemma 3.1, the sonic state can only be located on the side $z = z_R$ of the stationary wave. The opposite case $z_L > z_R$ can be treated as the mirror–image problem by reversing the Riemann initial data and setting the velocity in the opposite direction.

Here we study the general Riemann solution which contains a stationary wave. The sufficient condition for this requirement is that $u_{0L} > 0$ or $u_{0R} < 0$, where u_{0L} and u_{0R} were defined in (2.21) and (2.22). Otherwise if $u_{0L} < 0$ and $u_{0R} > 0$ the dry bed appears around the initial discontinuity point $x = x_0$. Specifically the solution has the wave configuration A_v; see Figure 1. Hereafter the symbols k–r, $k = 1, 2$ denote the k–rarefactions. An example of this case can be found in Figure 5. We can see that the jump of the bottom does not affect the motion of the flow. Therefore there is no stationary wave.

The general exact Riemann solution for the system (1.1) with (1.3) with $u_{0L} > 0$ or $u_{0R} < 0$ consists of a stationary wave which is located at $x = 0$ as well as a sequence of 1– and 2–shocks or rarefactions. Alcrudo and Benkhaldoun in [5] presented more than 20 different solution patterns. Indeed, the solution patterns without the dry bed under the condition (4.1) can be classified into 10 different wave configurations. We show them in Figures 2, 6, 8, 10, 12, 9, 14, 16, 17, and 18. In all of the wave configurations, the 1– and 2–wave represent a shock or a rarefaction. The dashed right arrow indicates that
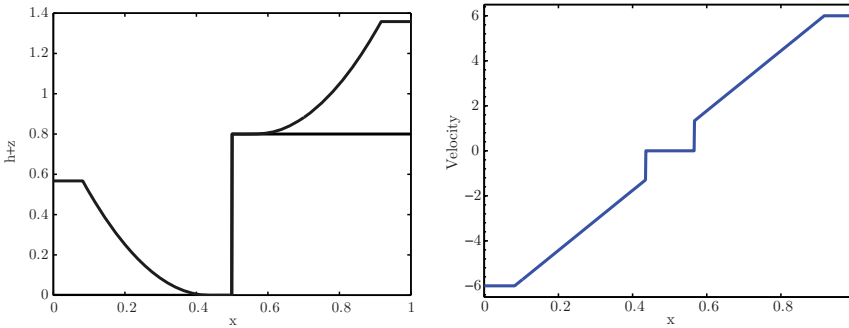
FIG. 5. Left: The water free surface $h + z$ at $t = 0.05$; Right: The velocity. The Riemann initial data are $(z_L, h_L, u_L) = (0.0, 0.5674, -6.0)$ when $x < 0.5$ and $(z_R, h_R, u_R) = (0.8, 0.558, 6.0)$ when $x > 0$.

the velocity across the bottom jump is positive, while the dashed left arrow indicates that the velocity across the bottom jump is negative. Note that the wave configuration E has been omitted by LeFloch and Thanh in [20].

The wave configurations A^T, C^T and D^T, in some sense, can be viewed as the image–reflection of the wave configurations A, C and D in terms of $x = 0$ respectively. Moreover, the wave configurations B and G contain a resonant wave due to the coincidence of the stationary wave with a 1– and 2–rarefaction wave respectively. The wave configurations C and C^T result from the coincidence of a stationary wave with a 0–speed 1– and 2–shock wave respectively, while the wave configurations E and F are the combination of a transonic rarefaction, a stationary wave and a 0–speed shock. We point out that analogous resonant waves to these mentioned here for other systems can be found in Goatin and LeFloch [15], Rochette and Clain [17], Han et al. [9] etc.

The solution patterns with a dry bed consist of the wave configurations A_v, H_1 and H_2; see Figures 1, 3, and 4 respectively. Also the wave configuration B_v, see Figure 7, belongs to this category. Note that the wave configuration B_v originated from the wave configuration B. But B_v contains a dry bed intermediate state $(0,0)$, and the 2–wave is a rarefaction wave. Here we should keep in mind that a 2–rarefaction wave will totally disappear if $h_R = 0$. This is analogous to the wave configurations D_v and E_v; see Figures 11 and 13, which comes from the wave configurations D and E respectively. The wave configuration G_v, see Figure 15, originated from the wave configuration G. Be advised that G_v contains a dry bed state $(0,0)$ and a 1–rarefaction if $h_L > 0$, or no 1–wave if $h_L = 0$. The situation for the wave configuration D_v^T, see Figure 19, is similar.

For one given set of initial data we cannot determine the wave configuration of the solution from the initial data in advance due to many possibilities of the mutual position between the stationary wave and shocks or rarefactions. This is the nature of a nonstrictly hyperbolic system. Analogous to the Euler equations in a duct, see Han et al. [9], we again introduce the L–M and R–M curves to solve this problem. We merge the stationary wave curve into the 1–wave curve $T_1(\mathbf{U}_L)$ or the 2–wave curve $T_2(\mathbf{U}_R)$. Here we also name them L–M and R–M curves. These two curves can be regarded as extensions of
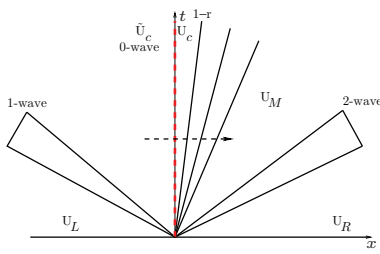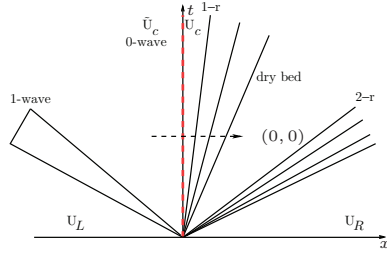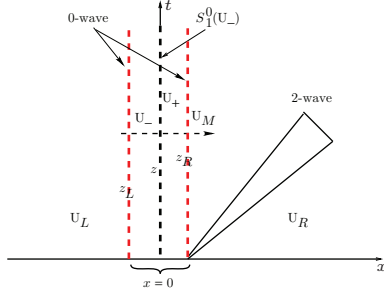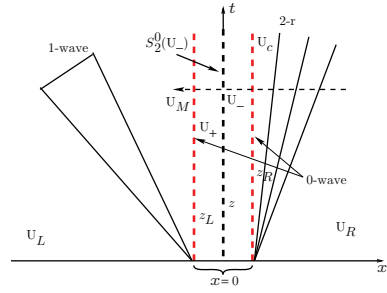
Fig. 6. B

Fig. 7. B_v
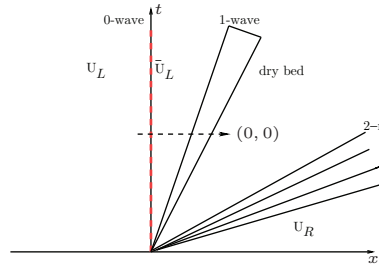

Fig. 8. C
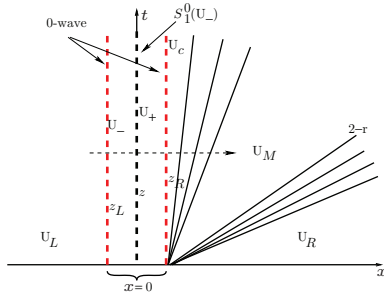

Fig. 9. F
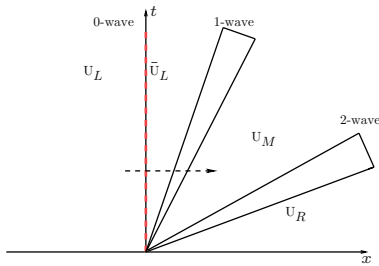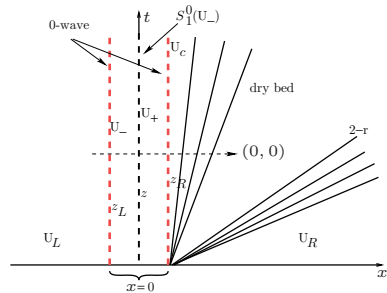

Fig. 10. D

Fig. 11. D_v

Fig. 12. E

Fig. 13. E_v

the $T_1(\mathbf{U}_L)$ and $T_2(\mathbf{U}_R)$ curves respectively. They will serve as building blocks for the calculation of the Riemann solutions to the shallow water equation in a uniform way.
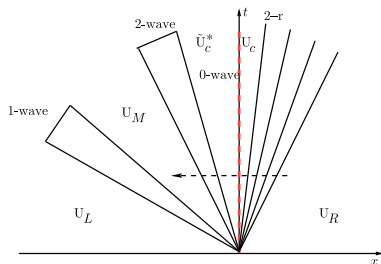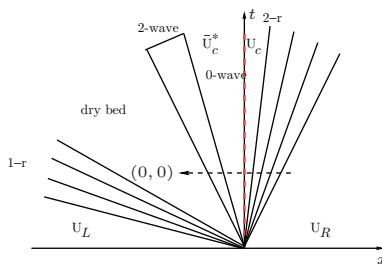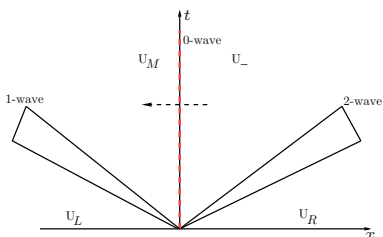
FIG. 14. G

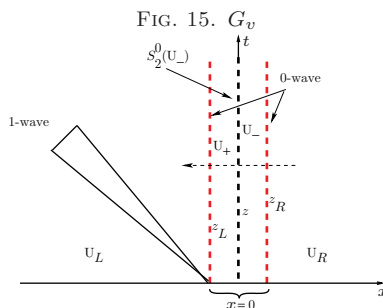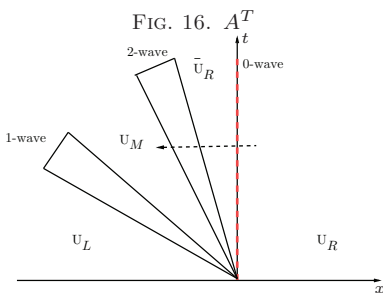FIG. 15. G_v

FIG. 16. A^T

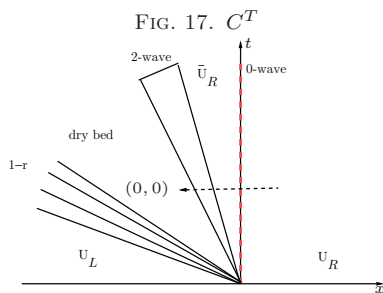
FIG. 17. C^T

FIG. 18. D^T

FIG. 19. D_v^T

There is precisely one stationary wave in a full wave curve from $\mathbf{U}_L$ to $\mathbf{U}_R$ located either on the L–M curve or the R–M curve. Due to the fact that the velocity does not change sign across the stationary wave, the location of the stationary wave is determined by this rule: If $u > 0$ the stationary wave is on the L–M curve; if $u < 0$ the stationary wave is on the R–M curve.

Hence if $u_{0L} > 0$ the L–M curve always contains the segment

$$P_1^l(\mathbf{U}_L) = \{\mathbf{U}|\mathbf{U} \in T_1(\mathbf{U}_L) \text{ with } u \leq 0\}; \tag{4.2}$$

otherwise if $u_{0L} \leq 0$ the L–M will be

$$P_1^l(\mathbf{U}_L) = \{\mathbf{U}|\mathbf{U} \in T_1(\mathbf{U}_L) \text{ with } u \leq u_{0L}\}. \tag{4.3}$$

Similarly if $u_{0R} < 0$ the R–M curve always contains the segment

$$P_1^r(\mathbf{U}_R) = \{\mathbf{U}|\mathbf{U} \in T_2(\mathbf{U}_R) \text{ with } u \geq 0\}; \tag{4.4}$$

otherwise if $u_{0R} \geq 0$ the R–M curve will be

$$P_1^r(\mathbf{U}_R) = \{\mathbf{U} | \mathbf{U} \in T_2(\mathbf{U}_R) \text{ with } u \geq u_{0R}\}. \tag{4.5}$$

It is necessary to construct the remaining segments of L–M curves with $u_{0L} > 0$ and $u > 0$, as well as for the R–M curves with $u_{0R} < 0$ and $u < 0$. Since $z_L < z_R$, Theorem 3.4 implies that the stationary wave always exists if the fluid flows from z_R to z_L. However the stationary wave equations (3.4) and (3.5) may not have solutions if the fluid flows from z_L to z_R. Before constructing the L–M and R–M curves, we need to consider the preliminaries for L–M and R–M curves first.

4.1. *Preliminaries for L–M curves with $u > 0$.* We now investigate the existence of the state $J(z_R; \mathbf{U}_-, z_L)$, where $\mathbf{U}_- \in T_1(\mathbf{U}_L)$ and is connected to $\mathbf{U}_L$ by a negative-speed 1–wave. Theorem 3.4 suggests the study of the following function

$$\omega(h_-) := h_- \left(\frac{1}{2} F(h_-)^2 - \frac{3}{2} F(h_-)^{\frac{2}{3}} + 1 \right) - (z_R - z_L), \tag{4.6}$$

where the Froude number $F(h_-) := \frac{U(h_-)}{\sqrt{gh_-}}$ and $U(h_-) = u_L - f(h_-; h_L)$. Theorem 3.4 implies that if $\omega(h_-) \geq 0$ the state $J(z_R; \mathbf{U}_-, z_L)$ exists and vice versa. So we need to study the behavior of $\omega(h_-)$.

LEMMA 4.1. *The function $\omega(h_-)$ is strictly increasing if $0 < F(h_-) < 1$.*

Proof. The function $\omega(h_-)$ is continuous and differentiable. The derivative of $\omega(h_-)$ is

$$\omega'(h_-) = \frac{1}{2} F(h_-)^2 - \frac{3}{2} F(h_-)^{\frac{2}{3}} + 1 + h_- F(h_-)^{-\frac{1}{3}} \left[F(h_-)^{\frac{4}{3}} - 1 \right] F'(h_-), \tag{4.7}$$

where by (2.19) and $U(h_-) > 0$, we have

$$F'(h_-) = -\frac{f'(h_-; h_L)}{\sqrt{gh_-}} - \frac{U(h_-)\sqrt{g}}{2} h_-^{-\frac{3}{2}} < 0.$$

As we have mentioned in (3.16), $\frac{1}{2} F(h_-)^2 - \frac{3}{2} F(h_-)^{\frac{2}{3}} + 1 \geq 0$. It takes the value 0 if and only if $F(h_-) = 1$. So we obtain that $\omega'(h_-) > 0$ if $0 < F(h_-) < 1$ and $\omega'(h_-) = 0$ if $F(h_-) = 1$. □

Denote the minimum value of h_- as h_L^{min} and the maximum as h_L^{max}. The curve $T_1(\mathbf{U}_L)$ is strictly decreasing in the (u, h) state space. Also, $\mathbf{U}_- \in T_1(\mathbf{U}_L)$ is connected to $\mathbf{U}_L$ by a negative-speed 1–wave. Hence if $u_L \leq c_L$, h_L^{min} is the height corresponding to the sonic state on the curve $T_1(\mathbf{U}_L)$; while if $u_L > c_L$, h_L^{min} is $\hat{h}_L$ which is defined in (2.12). That is to say we have

$$h_L^{min} = \begin{cases} \frac{(u_L + 2c_L)^2}{9g}, & \text{if } u_L \leq c_L, \\ \hat{h}_L, & \text{if } u_L > c_L. \end{cases} \tag{4.8}$$

Now we pay attention to h_L^{max}. It should satisfy

$$0 = u_L - f(h_-^{max}; \mathbf{U}_L). \tag{4.9}$$

If $u_L \leq 0$, we have $h_L^{max} < h_L$ which is the solution to the equation

$$u_L - 2(\sqrt{gh} - c_L) = 0.$$

This leads to $h_L^{max} = \frac{(u_L+2c_L)^2}{4g}$. Otherwise if $u_L > 0$, we have $h_L^{max} > h_L$. Hence from (2.16) it is the solution of the equation

$$u_L - (h - h_L)\sqrt{\frac{g}{2}\left(\frac{1}{h} + \frac{1}{h_L}\right)} = 0. \tag{4.10}$$

After a short calculation we have

$$\left(\frac{h}{h_L}\right)^3 - \left(\frac{h}{h_L}\right)^2 - (1 + 2F_L^2)\frac{h}{h_L} + 1 = 0. \tag{4.11}$$

Setting $x = \frac{h}{h_L} > 1$, (4.11) becomes

$$f(x) = x^3 - x^2 - (1 + 2F_L^2)x + 1. \tag{4.12}$$

Direct calculation yields the following facts. The function $f(x)$ defined in (4.12) reaches the maximum at $x_l := \frac{1}{3} - \frac{2}{3}\sqrt{1 + \frac{3}{2}F_L^2} < 0$ and the minimum at $x_r := \frac{1}{3} + \frac{2}{3}\sqrt{1 + \frac{3}{2}F_L^2} > 1$. When $x < x_l$, $f(x)$ increases from $-\infty$ to the maximum value at $x = x_l$. When $x \in]x_l, x_r[$, it decreases from the maximum value to the minimum value at $x = x_r$. When $x > x_r$, it increases from the minimum value to ∞. Furthermore, be advised that $x_l < 1 < x_r$ and $f(1) = -2F_L^2 < 0$, so $f(x_r) < f(1) < 0$. Thus there is exactly one real solution to the cubic equation $f(x) = 0$ when $x > x_r > 1$. We denote this solution as $x_{u_l^0}$ which can be directly calculated by the method for the exact solution to cubic equations; see Nickalls [8]. Finally we have

$$h_L^{max} = \begin{cases} \frac{(u_L+2c_L)^2}{4g}, & \text{if } u_L \leq 0, \\ h_L x_{u_l^0}, & \text{if } u_L > 0. \end{cases} \tag{4.13}$$

Thus the reasonable region for $\omega(h_-)$ is $]h_L^{min}, h_L^{max}[$. Moreover, we have the following lemma.

LEMMA 4.2. Set

$$z_{max} := z_L + h_L^{max}. \tag{4.14}$$

The stationary state $\mathbf{U} = J(z_R; \mathbf{U}_-, z_L)$ with $0 < u_- \leq c_-$ cannot exist if $z_{max} < z_R$.

Proof. Note that $\omega(h_L^{max}) = h_L^{max} - (z_R - z_L) = z_{max} - z_R$. So if $z_{max} < z_R$, $\omega(h_L^{max}) < 0$. The function $\omega(h_-)$ is increasing in terms of $h_- \in]h_L^{min}, h_L^{max}[$. Hence $\omega(h_L^{min}) < \omega(h_-) \leq \omega(h_L^{max}) < 0$ if $z_{max} < z_R$. Theorem 3.4 implies that if $\omega(h_-) < 0$, the stationary wave $\mathbf{U} = J(z_R; \mathbf{U}_-, z_L)$ cannot exist. $\square$

LEMMA 4.3. Suppose that $z_R < z_{max}$ and $u_L < c_L$. There exists a state $\tilde{\mathbf{U}}_c \in T_1(\mathbf{U}_L)$ which satisfies $\mathbf{U}_c = J(z_R; \tilde{\mathbf{U}}_c, z_L)$.

Proof. Due to $z_R < z_{max}$, we have $\omega(h_L^{max}) = z_{max} - z_L > 0$ and $h_L^{min} = \frac{(u_L+2c_L)^2}{9g}$. A short calculation yields that $\omega(h_L^{min}) = z_L - z_R < 0$. The function $\omega(h_-)$ is continuous and increasing. By the intermediate value theorem there is a unique solution to $\omega(h_-) = 0$. Denote the solution to $\omega(h_-) = 0$ as $\tilde{h}_c$. Then the corresponding velocity $\tilde{u}_c$ can be calculated by

$$\tilde{u}_c = u_L - f(\tilde{h}_c; \mathbf{U}_L). \tag{4.15}$$

The velocity function of $J(z_R; \tilde{\mathbf{U}}_c, z_L)$ is

$$\Psi(u; \tilde{\mathbf{U}}_c, z_L, z_R) := \frac{u^2}{2} + \frac{\tilde{c}_c^2 \tilde{u}_c}{u} - \frac{\tilde{u}_c^2}{2} - g\tilde{h}_c + g(z_R - z_L).$$

The minimum of this velocity function is

$$\Psi(u^*; \tilde{\mathbf{U}}_c, z_L, z_R) = g\omega(\tilde{h}_c) = 0.$$

Hence Remark 3.3 implies that the outflow state of stationary wave is a sonic state, i.e. $\mathbf{U}_c = J(z_R; \tilde{\mathbf{U}}_c, z_L)$. □

REMARK 4.4. Lemma 4.3 is totally consistent with Lemma 3.1.

Note that Lemma 4.2 states that in this case the flow coming from the left cannot spill over the obstacle caused by the jump in the bed height at $x = 0$, whereas in the case of Lemma 4.3, overspill occurs if the velocity is large enough, leading to $\omega(h_-) > 0$.

In the case when $z_R < z_{max}$ and $u_L > c_L$, we have $h_L^{min} = \hat{h}_L$. We define two critical bottom steps

$$z_S = z_L + \hat{h}_L \left(\frac{1}{2}\hat{F}_L^2 - \frac{3}{2}\hat{F}_L^{\frac{2}{3}} + 1 \right), \tag{4.16}$$

and

$$z_T = z_L + h_L \left(\frac{1}{2}F_L^2 - \frac{3}{2}F_L^{\frac{2}{3}} + 1 \right), \tag{4.17}$$

where $\hat{h}_L$ and $\hat{u}_L$ were defined in (2.12) and (2.13) respectively. The Froude number

$$\hat{F}_L = \frac{\hat{u}_L}{\hat{c}_L}. \tag{4.18}$$

Since $\hat{c}_L = \sqrt{g\hat{h}_L}$, taking (2.12) and (2.13) into (4.18), we obtain

$$\hat{F}_L = \frac{1}{8}F_L^{-2} \left[1 + \sqrt{1 + 8F_L^2} \right]^{\frac{3}{2}}. \tag{4.19}$$

We invoke the existence condition for resonant waves due to the coincidence of a 0–speed shock and the stationary wave.

LEMMA 4.5. Suppose $z_L < z_R < z_{max}$ and $u_L > c_L$. We have the following facts.
  (1) The state $\mathbf{U} = J(z_R; S_1^0(\mathbf{U}_L), z_L)$ exists if $z_R \leq z_S$; otherwise it fails to exist.
  (2) The state $\mathbf{U} = J(z_R; \mathbf{U}_L, z_L)$ exists if $z_R \leq z_T$; otherwise it fails to exist.
  (3) One always has $z_T > z_S$.

Proof. From Theorem 3.4 the existence condition for the state $\mathbf{U} = J(z_R; S_1^0(\mathbf{U}_L), z_L)$ is that

$$z_R \quad < \quad z_L + \hat{h}_L \left(\frac{1}{2}\left(\hat{F}_L\right)^2 - \frac{3}{2}\left(\hat{F}_L\right)^{\frac{2}{3}} + 1 \right) = z_S. \tag{4.20}$$

Analogously we can prove the second statement. Now we investigate the relationship between z_S and z_T. From (2.12) and (4.19), we have

$$z_S = z_L + h_L \left[\frac{1}{32F_L^2}\left(1 + \sqrt{1 + 8F_L^2}\right)^2 + \frac{-1 + \sqrt{1 + 8F_L^2}}{2} - \frac{3}{2}F_L^{\frac{2}{3}} \right]. \tag{4.21}$$

By (4.16) and (4.21), we have

$$
\begin{aligned}
z_T - z_S &= h_L \left[\frac{1}{2} F_L^2 - \frac{3}{2} F_L^{\frac{2}{3}} + 1 - \frac{1}{32 F_L^2} \left(1 + \sqrt{1 + 8F_L^2} \right)^2 - \frac{-1 + \sqrt{1 + 8F_L^2}}{2} + \frac{3}{2} F_L^{\frac{2}{3}} \right], \\
&= \frac{h_L}{F_L^2} \left[\frac{1}{2} F_L^4 + F_L^2 - \frac{1}{16} \left(1 + 4F_L^2 + \sqrt{1 + 8F_L^2} \right) - \frac{-1 + \sqrt{1 + 8F_L^2}}{2} F_L^2 \right], \\
&= \frac{h_L}{F_L^2} \left[\frac{1}{2} F_L^4 + \frac{5}{4} F_L^2 - \frac{1}{16} - \frac{\left(1 + 8F_L^2\right)^{\frac{3}{2}}}{16} \right], \\
&= \frac{h_L}{128 F_L^2} \left[-3 + \sqrt{1 + 8F_L^2} \right]^3 \left[1 + \sqrt{1 + 8F_L^2} \right]. \\
&> 0
\end{aligned}
$$

when $F_L^2 > 1$. $\qquad\qquad\qquad\qquad\qquad\qquad\qquad\qquad\qquad\qquad\qquad\qquad\square$

Assume that $z_L < z_R$ and $u_L > c_L$. We now consider resonant waves due to the coincidence of the 0–speed 1–shock with stationary waves. The 0–speed 1–shock splits the stationary wave into a supersonic part and a subsonic part. The corresponding wave curve is defined as follows.

$$
\left\{ \mathbf{U} | \mathbf{U} = \mathbf{J}(z_R; \mathbf{U}_+, z); \mathbf{U}_+ = S_1^0(\mathbf{U}_-); \mathbf{U}_- = \mathbf{J}(z; \mathbf{U}_L, z_L) \right\}, \tag{4.22}
$$

where $z \in]z_L, z_R[$. We denote the Froude numbers for the states $\mathbf{U}_\pm$ in (4.22) as $F_\pm = \frac{u_\pm}{\sqrt{gh_\pm}}$. By using (3.4) we have

$$
h_+ u_+ = h_- u_- = h_L u_L. \tag{4.23}
$$

Therefore we obtain the functions $F_\pm$ in terms of $h_\pm$ respectively:

$$
F(h_\pm) := F_\pm = \frac{u_L^2 h_L^2}{\sqrt{g} h_\pm^{\frac{3}{2}}}. \tag{4.24}
$$

By (4.23), the derivatives of the functions $F(h_\pm)$ are

$$
\frac{dF(h_\pm)}{dh_\pm} = -\frac{3}{2} \frac{F_\pm}{h_\pm}. \tag{4.25}
$$

Similar to (4.19), we obtain the further relations for F_- and F_+

$$
F_+ = \frac{1}{8} F_-^{-2} \left(1 + \sqrt{1 + 8F_-^2} \right)^{\frac{3}{2}}. \tag{4.26}
$$

The resonant wave curve in (4.22) is viewed as a function of z. Actually the variable h_- is more convenient to analyze the existence of the wave curve in (4.22). Specifically, the following lemma holds.

LEMMA 4.6. For the supersonic state $\mathbf{U}_- = \mathbf{J}(z; \mathbf{U}_L, z_L)$ in (4.22) with $z_L \leq z \leq z_R$, we have

$$
h_L \leq h_- \leq \bar{h}_L, \tag{4.27}
$$

where $\bar{\mathbf{U}}_L = \mathbf{J}(z_R; \mathbf{U}_L, z_L)$.

Proof. Considering (3.4) and (3.5) for $\mathbf{U}_- = \mathbf{J}(z; \mathbf{U}_L, z_L)$, we study the following equation:

$$\frac{h_L^2 u_L^2}{2gh_-^2} + h_- + z - \frac{u_L^2}{2g} - h_L - z_L = 0. \tag{4.28}$$

Taking z as a function of h_-, we obtain

$$z(h_-) := -\frac{h_L^2 u_L^2}{2gh_-^2} - h_- + \frac{u_L^2}{2g} + h_L + z_L. \tag{4.29}$$

Using (4.23), we have

$$\frac{dz(h_-)}{dh_-} = F_-^2 - 1 > 0. \tag{4.30}$$

Note that $h_- = h_L$ when $z = z_L$, while $h_- = \bar{h}_L$ when $z = z_R$. Thus (4.30) implies that $h_L \leq h_- \leq \bar{h}_L$. $\square$

To prove the existence of the wave curve defined in (4.22), we have to study the existence of the supersonic state $\mathbf{U}_- = \mathbf{J}(z; \mathbf{U}_L, z_L)$ and the subsonic state $\mathbf{U} = \mathbf{J}(z_R; \mathbf{U}_+, z)$ with $z_L \leq z \leq z_R$. We present the details in the following lemmas.

LEMMA 4.7. *The region of z for the existence of the subsonic state $\mathbf{U} = \mathbf{J}(z_R; \mathbf{U}_+, z)$ defined in (4.22) is as follows:*
(1) $z \in]z_L, z_R[$ *if* $z_S \geq z_R$;
(2) $z \in]z_c, z_R[$ *if* $z_S < z_R$ *where z_c is defined in (4.43).*

Proof. Theorem 3.4 implies that $\mathbf{U} = \mathbf{J}(z_R; \mathbf{U}_+, z)$ exists if

$$z_R - z \leq h_+ \left(\frac{1}{2} F_+^2 - \frac{3}{2} F_+^{\frac{2}{3}} + 1 \right). \tag{4.31}$$

In addition, by (2.12) and (2.13), we have

$$h_+ = \frac{h_-}{2} \left(-1 + \sqrt{1 + 8F_-^2} \right). \tag{4.32}$$

That is to say, h_+ can be treated as a function of h_-. This suggests to consider the function

$$\Theta(h_-) := h_+ \left(\frac{1}{2} F(h_+)^2 - \frac{3}{2} F(h_+)^{\frac{2}{3}} + 1 \right) + z - z_R. \tag{4.33}$$

For simplicity we introduce the function

$$A(h_+) := h_+ \left(\frac{1}{2} F(h_+)^2 - \frac{3}{2} F(h_+)^{\frac{2}{3}} + 1 \right).$$

Therefore $\Theta(h_-)$ in (4.33) can be rewritten as

$$\Theta(h_-) = A(h_+(h_-)) + z(h_-) - z_R. \tag{4.34}$$

By the chain rule we have

$$\Theta'(h_-) = \frac{dA(h_+)}{dh_+} \frac{dh_+}{dh_-} + \frac{dz(h_-)}{dh_-}. \tag{4.35}$$

Using (4.25) we obtain

$$\frac{dh_+}{dh_-} = -\frac{1}{2} + \frac{1 - 4F_-^2}{2\sqrt{1 + 8F_-^2}}. \tag{4.36}$$

Besides, by (4.25) and (4.26), we have

$$
\begin{aligned}
\frac{dA(h_+)}{dh_+} &= \frac{1}{2}F(h_+)^2 - \frac{3}{2}F(h_+)^{\frac{2}{3}} + 1 + h_+\left(F(h_+) - F(h_+)^{-\frac{1}{3}}\right)\frac{dF(h_+)}{dh_+} \\
&= \frac{1}{2}F(h_+)^2 - \frac{3}{2}F(h_+)^{\frac{2}{3}} + 1 - \frac{3}{2}F(h_+)\left(F(h_+) - F(h_+)^{-\frac{1}{3}}\right) \\
&= 1 - F(h_+) \\
&= 1 - \frac{1}{8}F_-^{-2}\left(1 + \sqrt{1 + 8F_-^2}\right)^{\frac{3}{2}}.
\end{aligned} \tag{4.37}
$$

By (4.30), (4.36) as well as (4.37), we have

$$
\begin{aligned}
\Theta'(h_-) &= \left(1 - \frac{1}{8}F_-^{-2}\left(1 + \sqrt{1 + 8F_-^2}\right)^{\frac{3}{2}}\right)\left(-\frac{1}{2} + \frac{1 - 4F_-^2}{2\sqrt{1 + 8F_-^2}}\right) + F_-^2 - 1 \\
&= \frac{\left(3 + \sqrt{1 + 8F_-^2}\right)\left[\left(-\frac{5}{2} + \sqrt{1 + 8F_-^2}\right)^2 + 2\left(1 + \sqrt{1 + 8F_-^2}\right)^{\frac{1}{2}} - \frac{17}{4}\right]}{8\sqrt{1 + 8F_-^2}}. \\
&> 0,
\end{aligned} \tag{4.38}
$$

when $F_-^2 > 1$. By Lemma 4.27, we have $h_L \le h_- \le \bar{h}_L$. Thus, due to (4.38), we have

$$
\Theta(h_L) \le \Theta(h_-) \le \Theta(\bar{h}_L). \tag{4.39}
$$

From (4.31), the state $\mathbf{J}(z_R; \mathbf{U}_+, z)$ exists if $\Theta(h_-) \ge 0$. Remember that we denote $\hat{\bar{\mathbf{U}}}_L = S_k^0(\bar{\mathbf{U}}_L)$. We have

$$
\Theta(\bar{h}_L) = \hat{\bar{h}}_L\left(\frac{1}{2}\hat{\bar{F}}_L^2 - \frac{3}{2}\hat{\bar{F}}_L^{\frac{2}{3}} + 1\right) \ge 0. \tag{4.40}
$$

From (4.16) as well as (4.33), we obtain that

$$
\Theta(h_L) = z_S - z_R. \tag{4.41}
$$

So, on one hand, if $z_S \ge z_R$, we have $0 \le \Theta(h_L) \le \Theta(h_-) \le \Theta(\bar{h}_L)$. Thus the state $\mathbf{J}(z_R; \mathbf{U}_+, z)$ exists for any $z_L \le z \le z_R$. On the other hand, if $z_S < z_R$, we have $\Theta(h_L) < 0 < \Theta(\bar{h}_L)$. From the intermediate value theorem there is a unique solution, denoted as $\tilde{h}_{c_s}$, to the equation $\Theta(h_-) = 0$ where $h_- \in]h_L, \bar{h}_L[$. The corresponding velocity can be calculated from

$$
\tilde{u}_{c_s} = \frac{h_L u_L}{\tilde{h}_{c_s}}, \tag{4.42}
$$

and the related bottom step denoted as z_c can be deduced from equation (4.28), i.e.

$$
z_c = -\frac{h_L^2 u_L^2}{2g\tilde{h}_{c_s}^2} + \tilde{h}_{c_s} - \frac{u_L^2}{2g} - h_L - z_L. \tag{4.43}
$$

Hence $\Theta(h_-) \ge 0$ if $z_c \le z \le z_R$. $\square$

LEMMA 4.8. Assume that $u_L > c_L$ for z_T, given by (4.17); we have $z_T < z_c$ if $z_T < z_R$.

Proof. Denote $\mathbf{U}_{c,l}^* = \mathbf{J}(z_R; \mathbf{U}_+, z_T)$. Taking $z = z_T$ in (4.28), we obtain that

$$\alpha(h_-) := \frac{h_L^2 u_L^2}{2h_-^2} + gh_- - \frac{3}{2}\left(u_L c_L^2\right)^{\frac{2}{3}} = 0. \tag{4.44}$$

The function $\alpha(h_-)$ is continuous and differentiable. The derivative of this function is

$$\alpha'(h_-) = -\frac{h_L^2 u_L^2}{h_-^3} + g. \tag{4.45}$$

Setting $h^* = h_L F_L^{\frac{2}{3}}$, we have $\alpha'(h_-) < 0$ if $h_- < h^*$, while $\alpha'(h_-) > 0$ if $h_- > h^*$. It has the minimum value at $h_- = h^*$ and $\alpha(h^*) = 0$. Therefore there is a unique solution to $\alpha(h_-) = 0$, i.e. $h_{c,l}^* = h^* = h_L F_L^{\frac{2}{3}}$. Using (4.23) we obtain that

$$u_{c,l}^* = u_L F_L^{-\frac{2}{3}} = c_L F_L^{\frac{1}{3}} = \sqrt{gh_{c,l}^*} = c_{c,l}^*.$$

Thus the state $\mathbf{U}_{c,l}^*$ is the sonic state. Hence we have $h^+ = h_{c,l}^*$ and $F^+ = 1$ in (4.32) and (4.24) respectively. From (4.6) we have $\Theta(h_{c,l}^*) = z_T - z_R < 0$ if $z_T < z_R$. Since $\Theta(\tilde{h}_{c_s}) = 0$, we have by (4.38) $h_{c,l}^* < \tilde{h}_{c_s}$. Consequently we have $z_T < z_c$ due to (4.29). $\qquad\square$

Based on Lemmas 4.6, 4.7, and 4.8, we now study the existence region for the wave curve defined in (4.22).

LEMMA 4.9. *Assume that $z_L < z_R$ and $u_L > c_L$; then we have*
  (1) *if $z_R \le z_S < z_T$, the curve in (4.22) exists.*
  (2) *if $z_S < z_R \le z_T$, the curve in (4.22) exists when $z \in]z_c, z_R[$.*
  (3) *if $z_S < z_T < z_R$, the curve in (4.22) fails to exist.*

Proof. The wave curve defined in (4.22) exists if the two states $\mathbf{U}_- = \mathbf{J}(z; \mathbf{U}_L, z_L)$ and $\mathbf{U} = \mathbf{J}(z_R; \mathbf{U}_+, z)$ exist. Lemma 4.5 implies that the state $\mathbf{U}_- = \mathbf{J}(z; \mathbf{U}_L, z_L)$ exists if $z \le z_T$.

Thus in one case when $z_R < z_T$, the state $\mathbf{U}_-$ defined in (4.22) with $z \in]z_L, z_R[$ always exists. Lemma 4.7 conveys that on one hand if $z_S \ge z_R$ the state $\mathbf{U} = \mathbf{J}(z_R; \mathbf{U}_+, z)$ exists when $z \in]z_L, z_R[$. Thus the first statement is true due to $z_S < z_T$ by Lemma 4.5. On the other hand, if $z_S < z_R$, the state $\mathbf{U} = \mathbf{J}(z_R; \mathbf{U}_+, z)$ exists when $z \in]z_c, z_R[$. This is the second statement.

In the other case when $z_R > z_T$, the state $\mathbf{U}_-$ exists if $z \in]z_L, z_T[$. By Lemmas 4.8 and 4.7 we have $]z_L, z_T[\bigcap]z_c, z_R[= \emptyset$. This is sufficient for the third statement. $\qquad\square$

REMARK 4.10. Suppose that we have $z_L < z_R$, $u_L > c_L$ and $z_S < z_R < z_T$. Lemma 4.9 reveals that there exists an $\tilde{h}_{c_s}$ such that $\Theta(\tilde{h}_{c_s}) = 0$. Moreover, note that $\Theta(\tilde{h}_{c_s})$ is the minimum value of the velocity function to $\mathbf{J}(z_R; \hat{\mathbf{U}}_{c_s}, z_c)$; i.e. the outflow state of $\mathbf{J}(z_R; \hat{\mathbf{U}}_{c_s}, z_c)$ is the sonic state. We denote it as $\mathbf{U}_{c_3}$, i.e. $\mathbf{U}_{c_3} = \mathbf{J}(z_R; \hat{\mathbf{U}}_{c_s}, z_c)$.

REMARK 4.11. Suppose $z_S < z_R < z_T$ and $u_L > c_L$, i.e. $h_L^{min} = \hat{h}_L$. Note that

$$\omega(\hat{h}_L) = z_S - z_R < 0. \tag{4.46}$$

Analogously to Lemma 4.3, there is a unique solution to $\omega(h_-) = 0$. Here we denote this as $\tilde{h}_c^L$. The corresponding velocity $\tilde{u}_c^L$ can be calculated from (4.15) by setting $\tilde{h}_c = \tilde{h}_c^L$.

Also we have $\mathbf{U}_{c_2} = J(z_R; \tilde{\mathbf{U}}_c, z_L)$, where $\mathbf{U}_{c_2}$ is the sonic state. The subscript 2 is used to distinguish the sonic state $\mathbf{U}_{c_2}$ from the sonic state $\mathbf{U}_{c_3}$ in Remark 4.10.

4.1.1. *Monotonicity.* In this section we consider the monotonicity of two types of curves as the preliminary step for the study of the L–M and R–M curves.

We define

$$P^l(\mathbf{U}_R) = \{\mathbf{U}|\mathbf{U} = \mathbf{J}(z_R; \mathbf{U}_-, z_L) \text{ and } \mathbf{U}_- \in T_1(\mathbf{U}_L) \} \tag{4.47}$$

where $h_L^{min} < h_- < h_L^{max}$ and

$$P^r(\mathbf{U}_R) = \{\mathbf{U}|\mathbf{U} = \mathbf{J}(z_L; \mathbf{U}_-, z_R) \text{ and } \mathbf{U}_- \in T_2(\mathbf{U}_R) \} \tag{4.48}$$

where $0 < u_- + c_- < c_-$. Note that $P^l(\mathbf{U}_L)$ and $P^r(\mathbf{U}_R)$ are the composites of the 1– or 2–wave curve with a stationary wave. Before studying the behavior of $P^l(\mathbf{U}_L)$ and $P^r(\mathbf{U}_R)$, we consider the following lemma first.

LEMMA 4.12. *For any state* $\mathbf{U}_- \in T_1(\mathbf{U}_L)$ *connected to* $\mathbf{U}_L$ *by a negative speed 1–wave, we have*

$$u_- - h_- f'(h_-; h_L) < 0, \quad \text{and} \quad u_- f'(h_-; h_L) - g < 0. \tag{4.49}$$

Proof. We have $u_- - c_- < 0$ since the states $\mathbf{U}_-$ and $\mathbf{U}_L$ are connected by a negative speed 1–wave. From (2.18) we have

$$u_- - h_- f'(h_-; h_L) = \begin{cases} u_- - c_-, & \text{if } h_- \leq h_L, \\ u_- - h_- \sqrt{\dfrac{g}{2}} \dfrac{\frac{1}{h_-} + \frac{2}{h_L} + \frac{h_L}{h_-^2}}{2\sqrt{\frac{1}{h_-} + \frac{1}{h_L}}}, & \text{if } h_- > h_L. \end{cases} \tag{4.50}$$

If $h_- \leq h_L$, obviously we have $u_- - h_- f'(h_-; h_L) < 0$. Otherwise if $h_- > h_L$, we have

$$\sqrt{\frac{g}{2}} \frac{\frac{1}{h_-} + \frac{2}{h_L} + \frac{h_L}{h_-^2}}{2\sqrt{\frac{1}{h_-} + \frac{1}{h_L}}} = \frac{\sqrt{g}}{2\sqrt{2}}\left(\sqrt{\frac{1}{h_-} + \frac{1}{h_L}} + \frac{\frac{1}{h_L} + \frac{h_L}{h_-^2}}{\sqrt{\frac{1}{h_-} + \frac{1}{h_L}}}\right)$$

$$\geq \sqrt{\frac{g}{2}}\sqrt{\frac{1}{h_L} + \frac{h_L}{h_-^2}} > \sqrt{\frac{g}{h_-}}. \tag{4.51}$$

So using (4.51) in (4.50), we obtain

$$u_- - h_- f'(h_-; h_L) \quad < \quad u_- - c_-. \tag{4.52}$$

Hence we have $u_- - h_- f'(h_-; h_L) < 0$ due to $u_- - c_- < 0$.

Now we turn to $u_- f'(h_-; h_L) - g$. Note that

$$u_- f'(h_-; h_L) - g = \begin{cases} \sqrt{\dfrac{g}{h_-}}(u_- - c_-) < 0, & \text{if } h_- \leq h_L, \\ u_- \sqrt{\dfrac{g}{2}} \dfrac{\frac{1}{h_-} + \frac{2}{h_L} + \frac{h_L}{h_-^2}}{2\sqrt{\frac{1}{h_-} + \frac{1}{h_L}}} - g, & \text{if } h_- > h_L. \end{cases} \tag{4.53}$$

So it is only necessary to consider the case that $h_- > h_L$. To ensure that the 1–wave has a negative speed, we have $h_- > h_-^{min}$ where

$$h_-^{min} = \begin{cases} h_L, & \text{if } u_L \leq c_L, \\ \hat{h}_L, & \text{if } u_L > c_L, \end{cases} \tag{4.54}$$

where $\hat{h}_L$ was defined in (2.12). Besides, by (2.20), we have

$$\frac{\partial u_- f_L'(h_-; h_L)}{\partial h_-} = -\left(f_L'(h_-; h_L)\right)^2 + u_- f_L''(h_-; h_L) < 0.$$

Therefore, when $h_- > h_L$, we have

$$u_- f_L'(h_-; h_L) < u_-^{min} f_L'(h_-^{min}; \mathbf{U}_L), \tag{4.55}$$

where $u_-^{min} = u_L - f(h_-^{min}; \mathbf{U}_L)$. Specifically, by (4.54), we have

$$u_- f'(h_-; h_L) - g < \begin{cases} u_L \sqrt{\dfrac{g}{h_L}} - g & \text{if } u_L \le c_L, \\[3mm] \hat{u}_L \sqrt{\dfrac{g}{2} \dfrac{\frac{1}{\hat{h}_L} + \frac{2}{h_L} + \frac{h_L}{\hat{h}_L^2}}{2\sqrt{\frac{1}{\hat{h}_L} + \frac{1}{h_L}}}} - g, & \text{if } u_L > c_L. \end{cases} \tag{4.56}$$

Note that when $u_L \le c_L$, $u_- f'(h_-; h_L) - g < \sqrt{\frac{g}{h_L}}(u_L - c_L) \le 0$. Now we consider the case when $u_L > c_L$. By $\hat{u}_L = \frac{h_L u_L}{\hat{h}_L}$, we have

$$\hat{u}_L \sqrt{\frac{g}{2} \frac{\frac{1}{\hat{h}_L} + \frac{2}{h_L} + \frac{h_L}{\hat{h}_L^2}}{2\sqrt{\frac{1}{\hat{h}_L} + \frac{1}{h_L}}}} = \frac{h_L u_L}{\hat{h}_L} \sqrt{\frac{g}{2} \frac{\frac{1}{\hat{h}_L} + \frac{2}{h_L} + \frac{h_L}{\hat{h}_L^2}}{2\sqrt{\frac{1}{\hat{h}_L} + \frac{1}{h_L}}}} = \frac{g}{2\sqrt{2}} F_L \frac{h_L}{\hat{h}_L} \frac{\left(\frac{h_L}{\hat{h}_L}\right)^2 + \frac{h_L}{\hat{h}_L} + 2}{\sqrt{\frac{h_L}{\hat{h}_L} + 1}}.$$

Moreover, from (2.12), we obtain that

$$\frac{h_L}{\hat{h}_L} = \frac{1 + \sqrt{1 + 8F_L^2}}{4F_L^2}.$$

Set $x = \frac{h_L}{\hat{h}_L}$. Then $F_L = \frac{\sqrt{x+1}}{\sqrt{2x}}$. So we have

$$\frac{g}{2\sqrt{2}} F_L \frac{h_L}{\hat{h}_L} \frac{\left(\frac{h_L}{\hat{h}_L}\right)^2 + \frac{h_L}{\hat{h}_L} + 2}{\sqrt{\frac{h_L}{\hat{h}_L} + 1}} = g\frac{x^2 + x + 2}{4} < g \qquad \text{by} \qquad 0 < x < 1.$$

Hence by (4.56), we obtain that $u_- f'(h_-; h_L) - g < 0$ when $u_L > c_L$. This completes the proof of the lemma. $\qquad\square$

THEOREM 4.13. *The curve $P^l(\mathbf{U}_L)$ defined in (4.47) is strictly decreasing in the (u, h) state plane, while $P^r(\mathbf{U}_R)$ defined in (4.48) is strictly increasing in the (u, h) state plane.*

Proof. It is sufficient to consider $P^l(\mathbf{U}_L)$. The other curve $P^r(\mathbf{U}_R)$ can be dealt with in an analogous way.

We need to prove that $\frac{du}{dh} < 0$. Due to $\mathbf{U} = \mathbf{J}(z_R; \mathbf{U}_-, z_L)$, we have

$$hu = h_- u_-, \tag{4.57}$$

$$\frac{u^2}{2} + g(h + z_R) = \frac{u^2}{2} + g(h_- + z_L), \tag{4.58}$$

where

$$u_- = u_L - f(h_-; h_L), \tag{4.59}$$

and $f(h_-; h_L)$ is defined in (2.16). By (4.57) and (4.58) we obtain the equations $\tau(h, h_-) = 0$ and $\varpi(u, h_-) = 0$, where

$$\tau(h, h_-) = \frac{(h_- u_-)^2}{2h^2} + g(h + z_R) - \frac{u_-^2}{2} - g(h_- + z_L) \tag{4.60}$$

and

$$\varpi(u, h_-) = \frac{u^2}{2} + g\left(\frac{h_- u_-}{u} + z_R\right) - \frac{u_-^2}{2} - g(h_- + z_L). \tag{4.61}$$

With the implicit function theorem we obtain

$$\frac{dh}{dh_-} = -\frac{\frac{\partial \tau}{\partial h_-}}{\frac{\partial \tau}{\partial h}} = \frac{\frac{\partial \tau}{\partial h_-}}{\frac{u^2 - c^2}{h}} \tag{4.62}$$

and

$$\frac{du}{dh_-} = -\frac{\frac{\partial \varpi}{\partial h_-}}{\frac{\partial \varpi}{\partial h}} = -\frac{\frac{\partial \varpi}{\partial h_-}}{\frac{u^2 - c^2}{u}}, \tag{4.63}$$

so we have

$$\frac{du}{dh} = \frac{\frac{du}{dh_-}}{\frac{dh}{dh_-}} = \frac{-u \frac{\partial \varpi}{\partial h_-}}{h \frac{\partial \tau}{\partial h_-}}. \tag{4.64}$$

Lemma 4.49 tells us that

$$\frac{\partial \tau}{\partial h_-} = \frac{h_- u_-}{h^2} u_- \left(u_- - h_- f'(h_-; h_L)\right) + u_- f'(h_-; h_L) - g < 0 \tag{4.65}$$

and

$$\frac{\partial \varpi}{\partial h_-} = \frac{g}{u} \left(u_- - h_- f'(h_-; h_L)\right) + u_- f'(h_-; h_L) - g < 0. \tag{4.66}$$

Hence we have $\frac{du}{dh} < 0$ from (4.64) by $h > 0$, $u > 0$. This completes the proof of the lemma. $\qquad\square$

Now we define the wave curve

$$P_{s0s}(\mathbf{U}_q) = \{\mathbf{U} | \mathbf{U} = \mathbf{J}(z_o; \mathbf{U}_+, z); \ \mathbf{U}_+ = S_0^k(\mathbf{U}_-); \ \mathbf{U}_- = \mathbf{J}(z; \mathbf{U}_q, z_i) \}, \tag{4.67}$$

where $u_q^2 \geq c_q^2$, $z_i \leq z \leq z_o$, as well as $k = 1$ when $u_q > 0$ while $k = 2$ when $u_q < 0$. The state $\mathbf{U}_- = \mathbf{J}(z; \mathbf{U}_q, z_i)$ is supersonic while $\mathbf{U} = \mathbf{J}(z_o; \mathbf{U}_+, z)$ is subsonic. Note that this type of resonant wave curve is the general case of the wave curve defined in (4.22). Moreover, we have the following monotonicity lemma for $P_{s0s}(\mathbf{U}_q)$.

LEMMA 4.14. Assume that $u_q^2 \geq c_q^2$; we have $\frac{dh}{dz} > 0$, while $\frac{du}{dz} > 0$ when $u_q > 0$ as well as $\frac{du}{dz} < 0$ when $u_q < 0$ for the wave curves in (4.67).

Proof. It is sufficient to consider the case that $k = 1$. The case for $k = 2$ can be dealt with in a similar way.

The curve $P_{s0s}(\mathbf{U}_q)$ defined in (4.67) is a function in terms of z. Note that $\frac{dh}{dz} = \frac{dh}{dh_-} \frac{dh_-}{dz}$. So we consider $\frac{dh}{dh_-}$ and $\frac{dh_-}{dz}$ in the following. Moreover, we have

$$h_q u_q = h_- u_- = h_+ u_+ = hu. \tag{4.68}$$

From $\mathbf{U}_- = \mathbf{J}(z; \mathbf{U}_q, z_i)$ and $\mathbf{U} = \mathbf{J}(z_o; \mathbf{U}_+, z)$, we respectively have

$$\frac{u_q^2 h_q^2}{2g h_-^2} + h_- + z - \frac{u_q^2}{2g} - h_q - z_i = 0 \tag{4.69}$$

and

$$\frac{u_q^2 h_q^2}{2gh^2} + h + z_o - \frac{(h_q u_q)^2}{2gh_+^2} - h_+ - z = 0, \tag{4.70}$$

where h_+ is defined in (4.32). Similarly to (4.29) and (4.30), we have

$$z(h_-) := -\frac{h_q^2 u_q^2}{2gh_-^2} - h_- + \frac{u_q^2}{2g} + h_q + z_q \tag{4.71}$$

and

$$\frac{dz(h_-)}{dh_-} = F_- - 1 > 0. \tag{4.72}$$

Taking (4.29) into (4.70), we introduce a equation $\xi(h, h_-) = 0$ where

$$\xi(h, h_-) = \frac{u_q^2 h_q^2}{2gh^2} + h + z_o - \frac{(h_q u_q)^2}{2gh_+^2} - h_+ - z(h_-). \tag{4.73}$$

So by the implicit function theorem we have

$$\frac{dh_-}{dh} = -\frac{\frac{\partial \xi}{\partial h}}{\frac{\partial \xi}{\partial h_-}} = \frac{F^2 - 1}{\frac{\partial \xi}{\partial h_-}} \tag{4.74}$$

where $F = \frac{u}{c}$. Using (4.26) and (4.37), we have

$$\begin{aligned}
\frac{\partial \xi}{\partial h_-} &= \frac{\partial \xi}{\partial h_+}\frac{dh_+}{dh_-} + \frac{\partial \xi}{\partial h_-} \\
&= (F_+^2 - 1)\frac{dh_+}{dh_-} - F_-^2 + 1 \\
&= -\Theta'(h_-) < 0. \tag{4.75}
\end{aligned}$$

So we obtain that $\frac{\partial \xi}{\partial h_-} < 0$ and $\frac{dh_-}{dh} > 0$. From (4.30) and (4.75), we obtain that $\frac{dh}{dz} = \frac{dh}{dh_-}\frac{dh_-}{dz} > 0$. Since $hu = h_q u_q$, $\frac{du}{dz} = -\frac{u}{h}\frac{dh}{dz}$. Hence $\frac{du}{dz} < 0$ if $u > 0$ and vice versa. $\square$

In the next section we study the L–M and R–M curves case by case. The gravity constant $g = 9.81$ unless otherwise stated.

4.2. *L–M curves with $u_{0L} > 0$ and $u > 0$.* There are five different types of L–M curves. We list the classification for all cases in the following:

- CASE I_L: $\quad z_{max} < z_R$.
- CASE II_L: $\quad z_{max} \geq z_R, u_L \leq c_L \Longleftrightarrow F_L < 1$.
- CASE III_L: $\quad z_{max} \geq z_R, u_L > c_L \Longleftrightarrow F_L > 1, z_R < z_S < z_T$.
- CASE IV_L: $\quad z_{max} \geq z_R, u_L > c_L \Longleftrightarrow F_L > 1, z_S < z_R < z_T$.
- CASE V_L: $\quad z_{max} \geq z_R, u_L > c_L \Longleftrightarrow F_L > 1, z_S < z_T < z_R$.

Later we will construct the L–M curves for all cases. Before doing this, we consider an example given by Andrianov in [3, (8)]. To match with the assumption $z_L < z_R$, we reflect the Riemann initial data with respect to $x = 0.5$. They become

$$(z, h, u) = \begin{cases} (1.1, 0.1, 2.0), & x < 0.5, \\ (1.5, 1.3, 2.0), & x > 0.5, \end{cases} \tag{4.76}$$

with $x \in [0, 1]$. Note that $g = 2$ in this example. For the given data $c_L = \sqrt{0.2}$, we have $u_L - c_L > 0$. From (4.14), we obtain $z_{max} = 1.7912$, $z_S = 1.3028$ and $z_T = 1.7928$. So

the L–M curve of this example belongs to CASE IV_L. Reducing z_R from 1.5 to 1.3, we obtain the Riemann initial data for CASE III_L. Later these Riemann initial data will be used to give examples for the Riemann solutions.

4.2.1. *CASE I_L: $z_{max} < z_R$.* This is the case when the jump of the bottom step is too high as compared with the inflow state $\mathbf{U}_-$ of the stationary wave, which is connected to $\mathbf{U}_L$ by a negative 1–wave. Mathematically we say that there is no solution to $J(z_R; \mathbf{U}_-, z_L)$ for any $\mathbf{U}_- \in T_1(\mathbf{U}_L)$ with a negative speed 1–wave. This was proved in Lemma 4.2.

Generally there are two different subcases for this case:

- $h_R = 0$.
- $u_{0R} > 0$.

We have the following two Riemann problems:

$$
\begin{aligned}
h_t + (hu)_x &= 0, \\
(hu)_t + (hu^2 + \tfrac{gh^2}{2})_x &= 0.
\end{aligned}
\tag{4.77}
$$

$$
(h, u)(x, 0) = \begin{cases} (h_L, u_L), & x < x_0, \\ (h_L, -u_L), & x > x_0. \end{cases}
\tag{4.78}
$$

$$
(h, u)(x, 0) = \begin{cases} (0, 0), & x < x_0, \\ (h_R, u_R), & x > x_0. \end{cases}
\tag{4.79}
$$

We find that when $h_R = 0$ or $u_{0R} > 0$, the solution of the Riemann problem can be split into two parts. One part is the solution to the Riemann problem (4.77) and (4.78) in the region $x < x_0$. The other part is the solution to Riemann problem (4.77) and (4.79) in the region $x > x_0$. Note that if $h_R = 0$, the solution to (4.77) and (4.79) is $h = 0$ and $u = 0$ for $(x, t) \in \mathbb{R} \times \mathbb{R}^+$. The wave configuration of $u_{0R} > 0$ can be seen in Figure 3. The wave configuration of $h_R = 0$ can refer to Figure 4.

Here we give two examples to illustrate our construction. The first example has the wave configuration H_1. The results are shown in Figure 20, where $z_{max} = 3.5769 < z_R = 4.7$. The second example has the wave configuration H_2. The results are shown in Figure 21, where $z_{max} = 2.4724 < z_R = 4.0$.
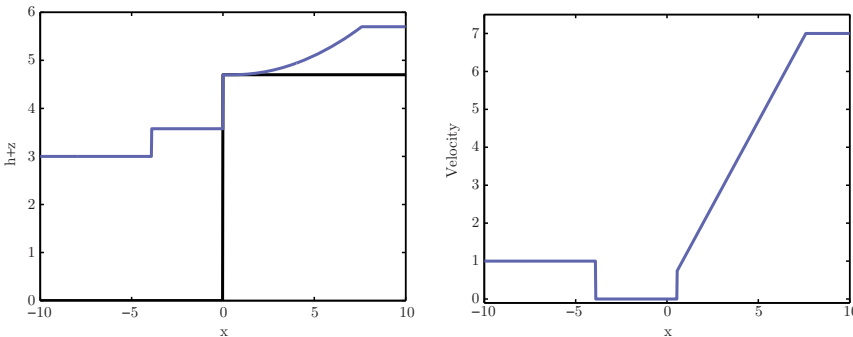

FIG. 20. Left: The water free surface $h + z$ at $t = 0.75$. Right: The velocity. The Riemann initial data are $(z_L, h_L, u_L) = (0, 3, 1)$ when $x < 0$ and $(z_R, h_R, u_R) = (4.7, 1.0, 7.0)$ when $x > 0$.
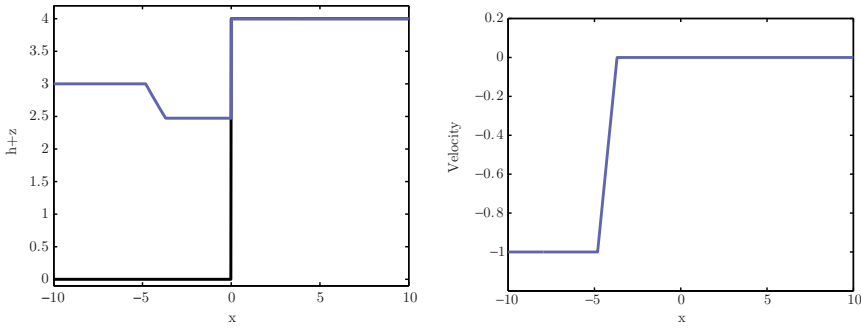
Fig. 21. Left: The water free surface $h + z$ at $t = 0.75$. Right: The velocity. The Riemann initial data are $(z_L, h_L, u_L) = (0, 3.0, -1.0)$ when $x < 0$ and $(z_R, h_R, u_R) = (4.0, 0, 0)$ when $x > 0$.

4.2.2. *CASE II_L: $z_{max} \geq z_R$, $u_L \leq c_L$.* In this case the L–M curve consists of three segments which are defined as follows:

$$P_1^l(\mathbf{U}_L) = \{\mathbf{U} | \mathbf{U} \in T_1(\mathbf{U}_L) \text{ with } u < 0\},$$
$$P_2^l(\mathbf{U}_L) = \{\mathbf{U} | \mathbf{U} = \mathbf{J}(z_R; \mathbf{U}_-, z_L) \text{ and } \mathbf{U}_- \in T_1(\mathbf{U}_L) \text{ with } 0 < u_- < \tilde{u}_c, \ 0 < u < u_c\},$$
$$P_3^l(\mathbf{U}_L) = \{\mathbf{U} | \mathbf{U} \in T_1(\mathbf{U}_c) \text{ with } u > u_c\},$$

where $\mathbf{U}_c = \mathbf{J}(z_R; \tilde{\mathbf{U}}_c, z_L)$, $\tilde{\mathbf{U}}_c \in T_1(\mathbf{U}_L)$ which is defined in (4.15).

The continuity of the three segments is obvious. According to Theorem 4.13, the segment $P_2^l(\mathbf{U}_L)$ is strictly decreasing in the $(u, h + z)$ space. Also the segments $P_1^l(\mathbf{U}_L)$ and $P_3^l(\mathbf{U}_L)$ are strictly decreasing in the $(u, h + z)$ space due to Lemma 2.1. So the L–M curve $\bigcup_{k=1}^{3} P_k^l(\mathbf{U}_L)$ is strictly decreasing in the $(u, h + z)$ space.

We define

$$u_{0L}^* = 3u_c. \tag{4.80}$$

If $u_{0L}^* > u_{0R}$, there is a unique intersection point between the L–M curve and the R–M curve. If the intersection point lies on the segment $P_2^l(\mathbf{U}_L)$, the solution has the wave configurations A; see Figure 2. Here we use an example given by Alcrudo and Benkhaldoun in [5] to illustrate the corresponding L–M curve and the exact free surface of the fluids, as well as the Froude number in Figure 22. If the intersection point lies on the segment $P_3^l(\mathbf{U}_L)$, the solution has the wave configuration B. An example is shown in Figure 23. We observe that the Froude number is greater than 1 when the water goes across the bottom jump.

Otherwise if $u_{0L}^* < u_{0R}$ and $h_R > 0$, the Riemann solution contains a dry bed state and behaves in the manner of the wave configuration B_v; see Figure 7. The example for $h_R > 0$ is shown in Figure 24. The example for $h_R = 0$ is shown in Figure 25.
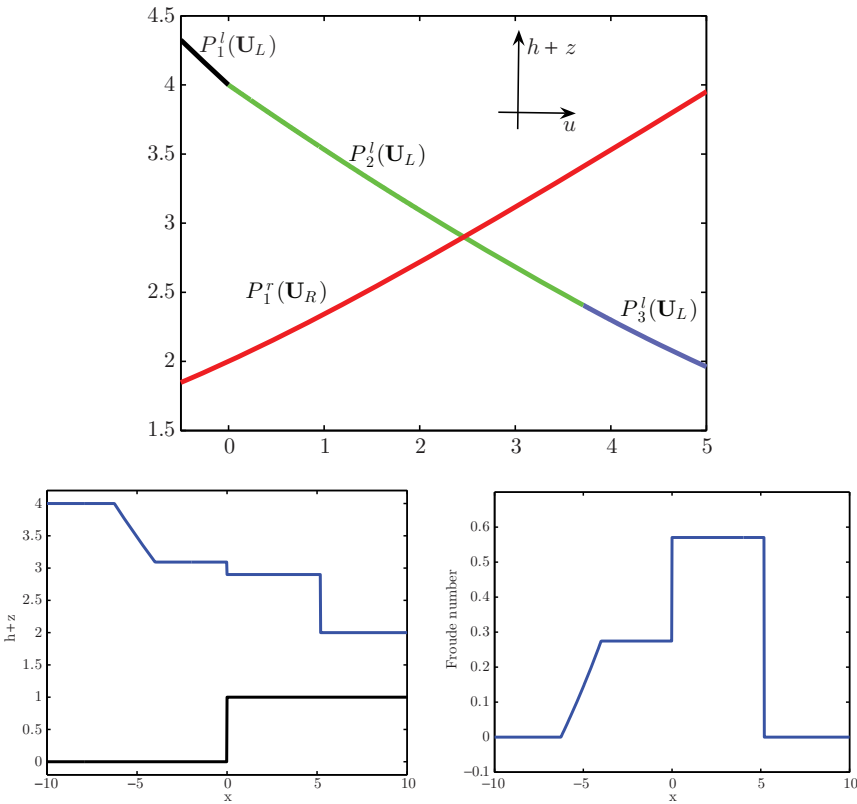
Fig. 22. Top: L–M curve $\bigcup_{k=1}^{3} P_k^l(\mathbf{U}_L)$. Bottom left: The water free surface $h + z$ at $t = 1.0$. Bottom right: The Froude number. The Riemann initial data are $(z_L, h_L, u_L) = (0.0, 4.0, 0.0)$ when $x < 0$ and $(z_R, h_R, u_R) = (1.0, 1.0, 0.0)$ when $x > 0$.

4.2.3. *CASE III$_L$*: $z_{max} \geq z_R$, $u_L > c_L$, $z_R < z_S < z_T$. In this case the L–M curve consists of the following four parts:

$P_1^l(\mathbf{U}_L) = \{\mathbf{U} | \mathbf{U} \in T_1(\mathbf{U}_L) \text{ with } u < 0\}$,
$P_2^l(\mathbf{U}_L) = \{\mathbf{U} | \mathbf{U} = \mathbf{J}(z_R; \mathbf{U}_-, z_L) \text{ and } \mathbf{U}_- \in S_1^-(\mathbf{U}_L) \text{ with } 0 < u_- < \hat{u}_L, \ 0 < u < \bar{\hat{u}}_L\}$,
$P_3^l(\mathbf{U}_L) = \{\mathbf{U} | \mathbf{U} = \mathbf{J}(z_R; \mathbf{U}_+, z); \ \mathbf{U}_+ = S_1^0(\mathbf{U}_-); \ \mathbf{U}_- = \mathbf{J}(z; \mathbf{U}_L, z_L), z_L \leq z \leq z_R\}$,
$P_4^l(\mathbf{U}_L) = \{\mathbf{U} | \mathbf{U} \in T_1(\bar{\mathbf{U}}_L) \text{ with } u > \bar{\hat{u}}_L\}$,

where $\bar{\hat{\mathbf{U}}}_L = \mathbf{J}(z_R; \hat{\mathbf{U}}_L, z_L)$ and $\hat{\mathbf{U}}_L = S_1^0(\mathbf{U}_L)$, while $\bar{\hat{\mathbf{U}}}_L = S_1^0(\bar{\mathbf{U}}_L)$ and $\bar{\mathbf{U}}_L = \mathbf{J}(z_R; \mathbf{U}_L, z_L)$. Due to $z_L < z_R$, Lemma 4.14 tells us that h is increasing while u is decreasing when z varies monotonically from z_L to z_R. So $\bar{\hat{h}}_L < \bar{\hat{h}}_L$ and $\bar{\hat{u}}_L > \bar{\hat{u}}_L$. As shown in Figure 26, the L–M curve is folding in the $(u, h + z)$ state space.

We define

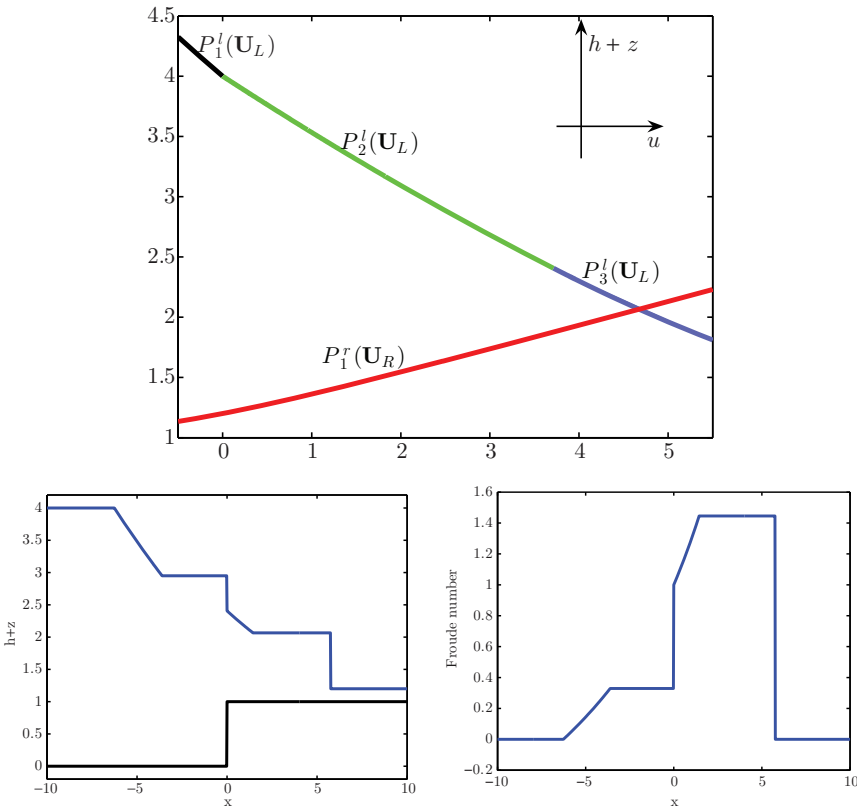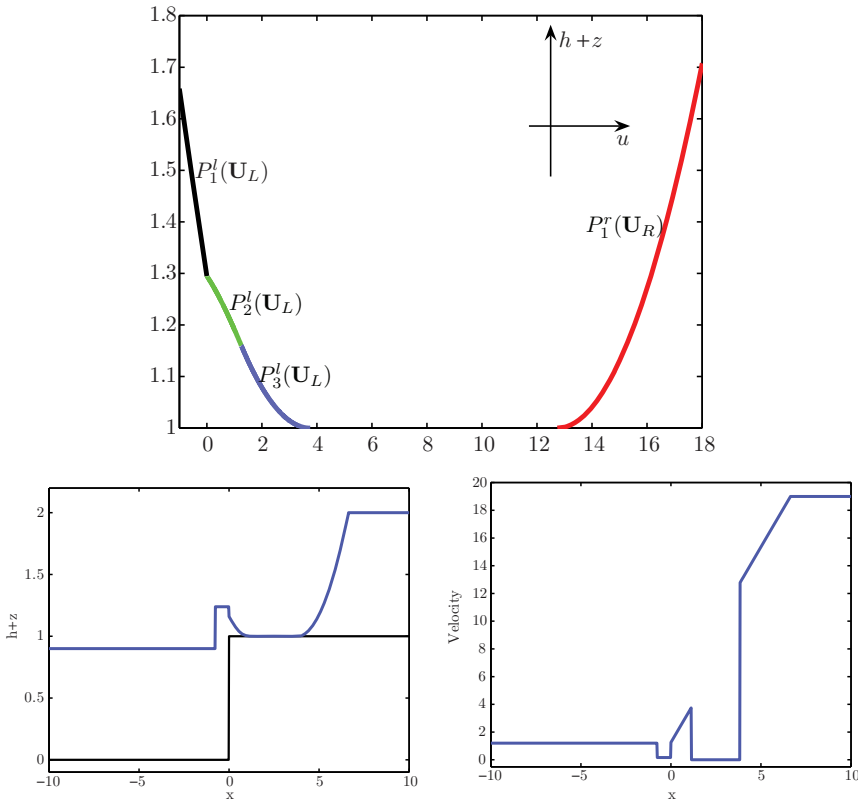$$u_{0L}^* = \bar{u}_L + 2\bar{c}_L. \tag{4.81}$$

FIG. 23. Top: L–M curve $\bigcup_{k=1}^{3} P_k^l(\mathbf{U}_L)$. Bottom left: The water free surface $h + z$ at $t = 1.0$. Bottom right: The Froude number. The Riemann initial data are $(z_L, h_L, u_L) = (0.0, 4.0, 0.0)$ when $x < 0$ and $(z_R, h_R, u_R) = (1.0, 0.2, 0.0)$ when $x > 0$.

Note that if $u_{0L}^* > u_{0R}$, there are intersection points between the L–M curve and the R–M curve. If the intersection point lies on the segment $P_2^l(\mathbf{U}_L)$, the solution is in the pattern of the wave configuration A. This is analogous to the CASE II_L. If the intersection point lies on the segment $P_3^l(\mathbf{U}_L)$, the solution has the wave configuration C, while if the intersection point lies on the segment $P_4^l(\mathbf{U}_L)$, the solution has the wave configuration D.

Due to the fact that the L–M curve is folding in the $(u, h + z)$ state space, if the intersection point lies on the segment $P_3^l(\mathbf{U}_L)$, we can also find two other intermediate states lying on the segments $P_2^l(\mathbf{U}_L)$ and $P_4^l(\mathbf{U}_L)$ respectively. So for one set of given initial data, there are three solutions with wave configurations A, C and D respectively. An example with $g = 2.0$ is shown in Figure 26. An example for $g = 9.81$ is shown in Figure 27.

FIG. 24. Top: L–M curve $\bigcup\limits_{k=1}^{3} P_k^l(\mathbf{U}_L)$. Bottom left: The water free surface $h + z$ at $t = 0.3$. Bottom right: The velocity. The Riemann initial data are $(z_L, h_L, u_L) = (0, 0.9, 1.2)$ when $x < 0$ and $(z_R, h_R, u_R) = (1.0, 1.0, 19.0)$ when $x > 0$.

Moreover, if $u_{0L}^* < u_{0R}$, the solution with the wave configuration D_v occurs. An example for $h_R > 0$ is shown in Figure 28. An example for $h_R = 0$ is shown in Figure 29. Note that the computational region for these two examples is $[-10, 10]$ and $g = 2.0$.

4.2.4. *CASE IV_L*: $z_{max} \geq z_R$, $u_L > c_L$, $z_S < z_R < z_T$. In this case the L–M curve consists of six parts. They are defined as follows:

$$
\begin{aligned}
P_1^l(\mathbf{U}_L) &= \{\mathbf{U} | \mathbf{U} \in T_1(\mathbf{U}_L) \text{ with } u < 0\}, \\
P_2^l(\mathbf{U}_L) &= \{\mathbf{U} | \mathbf{U} = \mathbf{J}(z_R; \mathbf{U}_-, z_L) \text{ and } \mathbf{U}_- \in S_1^-(\mathbf{U}_L) \text{ with } u_- < \tilde{u}_c^L, u < u_{c_2}\}, \\
P_3^l(\mathbf{U}_L) &= \{\mathbf{U} | \mathbf{U} = \mathbf{J}(z_R; \mathbf{U}_+, z); \ \mathbf{U}_+ = S_0(\mathbf{U}_-); \ \mathbf{U}_- = \mathbf{J}(z; \mathbf{U}_L, z_L), z_c \leq z \leq z_R\}, \\
P_4^l(\mathbf{U}_L) &= \{\mathbf{U} | \mathbf{U} \in T_1(\bar{\mathbf{U}}_L) \text{ with } u > \hat{\bar{u}}_L\}, \\
P_5^l(\mathbf{U}_L) &= \{\mathbf{U} | \mathbf{U} \in T_1(\mathbf{U}_{c_2}) \text{ with } u > u_{c_2}\}, \\
P_6^l(\mathbf{U}_L) &= \{\mathbf{U} | \mathbf{U} \in T_1(\mathbf{U}_{c_3}) \text{ with } u > u_{c_3}\},
\end{aligned}
$$

where $(\tilde{h}_c^L, \tilde{u}_c^L)$ and $\mathbf{U}_{c_2}$ are defined in Remark 4.10, while $\mathbf{U}_{c_3}$ is defined in Remark 4.11. Compared with the L–M curve in CASE III_L, it seems that the boundary state
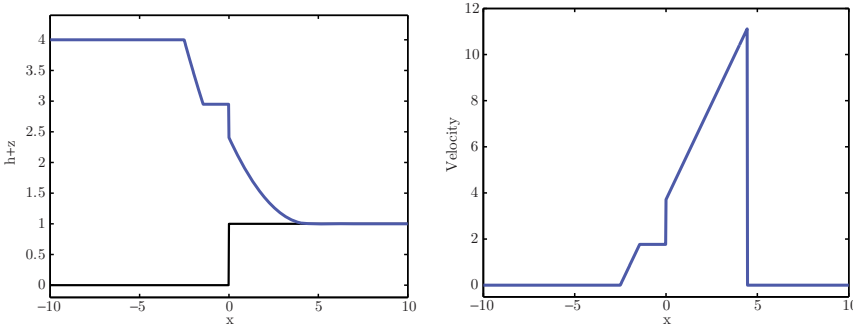
FIG. 25. Left: The water free surface $h + z$ at $t = 0.4$. Right: The velocity. The Riemann initial data are $(z_L, h_L, u_L) = (0, 4.0, 0.0)$ when $x < 0$ and $(z_R, h_R, u_R) = (1.0, 0.0, 0.0)$ when $x > 0$.

$\hat{\mathbf{U}}_L$ bifurcates into two segments $P_5^l(\mathbf{U}_L)$ and $P_6^l(\mathbf{U}_L)$. Generally the L–M curve in this case consists of three branches $P_1^l(\mathbf{U}_L) \cup P_2^l(\mathbf{U}_L) \cup P_5^l(\mathbf{U}_L)$, $P_3^l(\mathbf{U}_L) \cup P_6^l(\mathbf{U}_L)$ and $P_4^l(\mathbf{U}_L)$; see Figure 31. Apparently, if the intersection points belong to $P_3^l(\mathbf{U}_L)$, $P_4^l(\mathbf{U}_L)$, $P_5^l(\mathbf{U}_L)$ or $P_6^l(\mathbf{U}_L)$, there are three possible solutions for the same initial data.

Analogously to CASE III_L, the wave configurations A, C and D are related to the segments $P_2^l(\mathbf{U}_L)$, $P_3^l(\mathbf{U}_L)$ and $P_4^l(\mathbf{U}_L)$ respectively. Besides, the wave configuration B is related to the segment $P_5^l(\mathbf{U}_L)$, while the wave configuration E, see Figure 12, is related to the segment $P_6^l(\mathbf{U}_L)$.

An example of the three solutions with the wave configurations A, C and D is presented in Figure 31. As we have mentioned, this example comes from Andrianov [3]. However, he omitted the solution with the wave configuration C due to the fact that it contains a resonant wave $S0S(\mathbf{U_L})$; see [9]. We reduce h_R in (4.76) from 1.3 to 0.45. There are still three solutions but with the wave configurations B, E and F; see Figure 30.

We define

$$u_{0L}^{*,1} = 3u_{c_2}, \quad u_{0L}^{*,2} = 3u_{c_3}, \quad u_{0L}^{*,3} = \bar{u}_L + 2\bar{c}_L. \tag{4.82}$$

Note that if $u_{0L}^{*,1} < u_{0R}$, a solution with the wave configuration B_v occurs. Similarly, if $u_{0L}^{*,2} < u_{0R}$, a solution with the wave configuration E_v occurs, while if $u_{0L}^{*,3} < u_{0R}$, the solution with the wave configuration D_v occurs. The example of these three types of solutions with $h_R > 0$ can be found in Figure 32. The example for the case when $h_R = 0$ is shown in Figure 33.

4.2.5. *CASE V_L*: $z_{max} \geq z_R$, $u_L > c_L$, $z_S < z_T < z_R$. When $z_T < z_S < z_R$, Lemma 4.9 tells us the segment $P_3^l(\mathbf{U}_L)$ in (4.22) fails to exist. Therefore the L–M curve in this case consists of three segments, which are defined as follows:

$$
\begin{array}{rcl}
P_1^l(\mathbf{U}_L) & = & \{\mathbf{U} | \mathbf{U} \in T_1(\mathbf{U}_L) \text{ with } u < 0\}, \\
P_2^l(\mathbf{U}_L) & = & \{\mathbf{U} | \mathbf{U} = \mathbf{J}(z_R; \mathbf{U}_-, z_L) \text{ and } \mathbf{U}_- \in S_1^-(\mathbf{U}_L) \text{ with } u_- < \tilde{u}_c^L, u < u_{c_2}\}, \\
P_3^l(\mathbf{U}_L) & = & \{\mathbf{U} | \mathbf{U} \in T_1(\mathbf{U}_{c_2}) \text{ with } u > u_{c_2}\}.
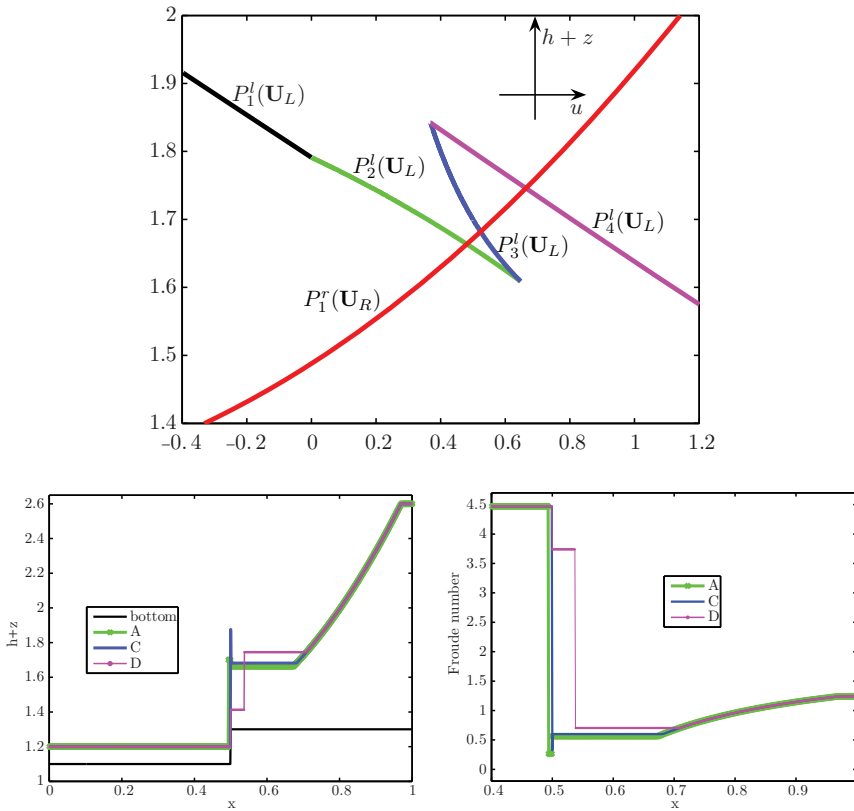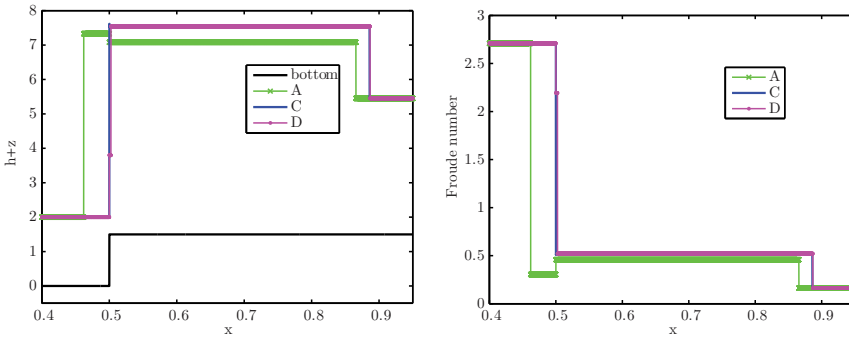\end{array}
$$

Fig. 26. Top: L–M curve $\bigcup_{k=1}^{4} P_k^l(\mathbf{U}_L)$. Bottom left: The water free surface $h + z$ at $t = 0.13$. Bottom right: The Froude number. The Riemann initial data are given in (4.76) but with $z_R = 1.3$.

Note that the L–M curve in this case is just one branch of the L–M curve in CASE IV_L and it is decreasing and continuous. We define

$$u_{0L}^* = 3u_{c_2}. \tag{4.83}$$

We observe that if $u_{0L}^* > u_{0R}$, there is an intersection point between the L–M curve and the R–M curve. If the intersection point lies on $P_2^l(\mathbf{U}_L)$, the solution has the wave configuration A. An example is shown in Figure 34. In the other case when the intersection point lies on $P_2^l(\mathbf{U}_L)$, the solution has the wave configuration B. An example is shown in Figure 35. In the other case when $u_{0L}^* < u_{0R}$, the solution with the wave configuration B_v occurs. An example with $h_R > 0$ is shown in Figure 36. An example with $h_R = 0$ is shown in Figure 37.

4.3. *R–M curves with $u_{0R} < 0$ and $u < 0$.* Generally, there are two possible cases for the R–M curves if $z_L < z_R$. Remember that we do not have to consider $z_R > z_L$ because these cases can be deduced by symmetry of solutions.

- CASE I_R: $u_R + c_R \geq 0 \Longleftrightarrow F_R > -1$.

FIG. 27. Left: The water free surface $h + z$ at $t = 0.03$. Right: The Froude number. The Riemann initial data are $(z_L, h_L, u_L) = (0, 2.0, 12.0)$ when $x < 0.5$ and $(z_R, h_R, u_R) = (1.5, 3.9524, 1.0142)$ when $x > 0.5$. The computational region is $[0.4, 0.95]$.
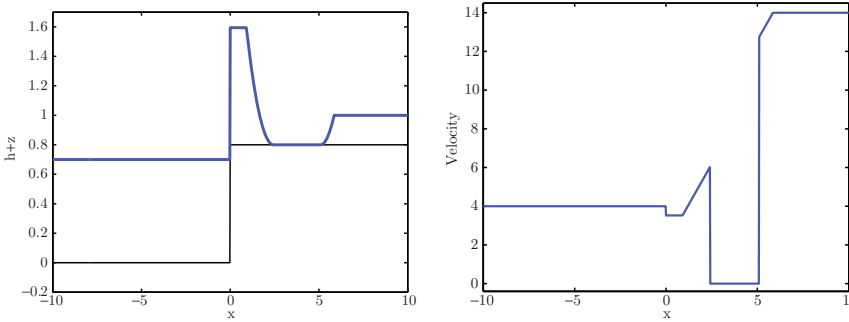

FIG. 28. Left: The water free surface $h + z$ at $t = 0.4$. Right: The velocity. The Riemann initial data are $(z_L, h_L, u_L) = (0, 0.7, 4.0)$ when $x < 0$ and $(z_R, h_R, u_R) = (0.8, 0.2, 14.0)$ when $x > 0$.

• CASE II_R: $u_R + c_R < 0 \iff F_R < -1$.
We define h_R^{max} as the solution to equation

$$0 = u_R + f(h_R^{max}; h_R). \tag{4.84}$$

The calculation procedure for h_R^{max} is similar to h_L^{max} in (4.13). We intend to study these two cases of the R–M curves in the following.

4.3.1. *CASE I_R: $u_R + c_R \geq 0$.* In this case the sonic state can only appear on the right side of the initial discontinuity located at $x = x_0$ due to the fact that $z_L < z_R$, i.e. $\mathbf{U}_c \in T_2(\mathbf{U}_R)$. According to Remark 3.3, $\mathbf{U} = \mathbf{J}(z_R; \mathbf{U}_c, z_L)$ has two solutions. One is supersonic, and the other one is subsonic. We use $\bar{\mathbf{U}}_c^* = \mathbf{J}(z; \mathbf{U}_c, z_R)$ to denote the supersonic one and $\bar{\mathbf{U}}_c = \mathbf{J}(z; \mathbf{U}_c, z_R)$ to denote the subsonic one.
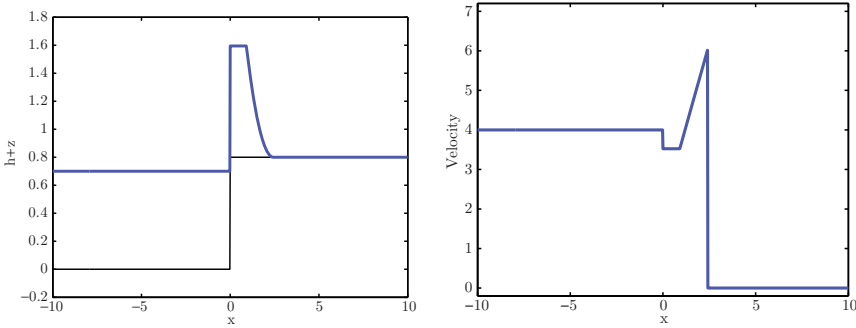
FIG. 29. Left: The water free surface $h + z$ at $t = 0.4$. Right: The velocity. The Riemann initial data are $(z_L, h_L, u_L) = (0, 0.7, 4.0)$ when $x < 0$ and $(z_R, h_R, u_R) = (0.8, 0, 0)$ when $x > 0$.
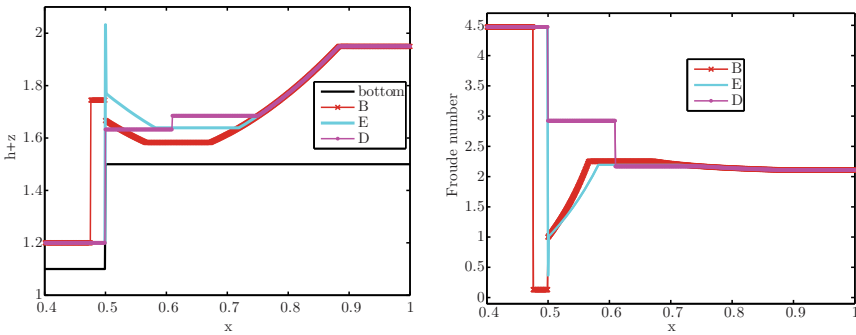

FIG. 30. Left: The water free surface $h + z$ at $t = 1$. Right: The Froude number. The Riemann initial data are given in (4.76) but with $h_R = 0.45$.

The R–M curve in this case consists of four segments, which are defined in the following:

$$P_1^r(\mathbf{U}_R) = \left\{ \mathbf{U} | \mathbf{U} \in T_2(\mathbf{U}_R) \text{ with } u > 0 \right\},$$
$$P_2^r(\mathbf{U}_R) = \left\{ \mathbf{U} | \mathbf{U} = \mathbf{J}(z_L; \mathbf{U}_-, z_R) \text{ and } \mathbf{U}_- \in T_2(\mathbf{U}_R) \text{ with } u_c < u_- < 0, \ \bar{u}_c < u < 0 \right\},$$
$$P_3^r(\mathbf{U}_R) = \left\{ \mathbf{U} | \mathbf{U} = \mathbf{J}(z_L; \mathbf{U}_+, z); \ \mathbf{U}_+ = S_2^0(\mathbf{U}_-); \ \mathbf{U}_- = \mathbf{J}(z; \mathbf{U}_c, z_R), z_L \leq z \leq z_R \right\},$$
$$P_4^r(\mathbf{U}_L) = \left\{ \mathbf{U} | \mathbf{U} \in T_2(\bar{\mathbf{U}}_c^*) \text{ with } u < \hat{\bar{u}}_c \right\}.$$

(4.85)

We have to remember that the state $\mathbf{U} = \mathbf{J}(z_R; \mathbf{U}_+, z)$ is subsonic, and the state $\mathbf{U}_- = \mathbf{J}(z; \mathbf{U}_c, z_L)$ is supersonic for the segment $P_3^r(\mathbf{U}_R)$.

The continuity of the three segments is obvious. From Lemma 2.1 the segments of $P_1^r(\mathbf{U}_R)$ and $P_4^r(\mathbf{U}_R)$ are strictly increasing in the $(u, h+z)$ space. Theorem 4.13 indicates that $P_2^r(\mathbf{U}_R)$ is strictly increasing in the $(u, h + z)$ space. Moreover, due to the fact that $z_L < z_R$, Lemma 4.14 tells us that h and u are strictly decreasing when z varies from z_R to z_L. So the segment $P_3^r(\mathbf{U}_R)$ is strictly increasing in the $(u, h + z)$ space. In summary, the R–M curve in this case is continuous and strictly increasing in the $(u, h + z)$ space.
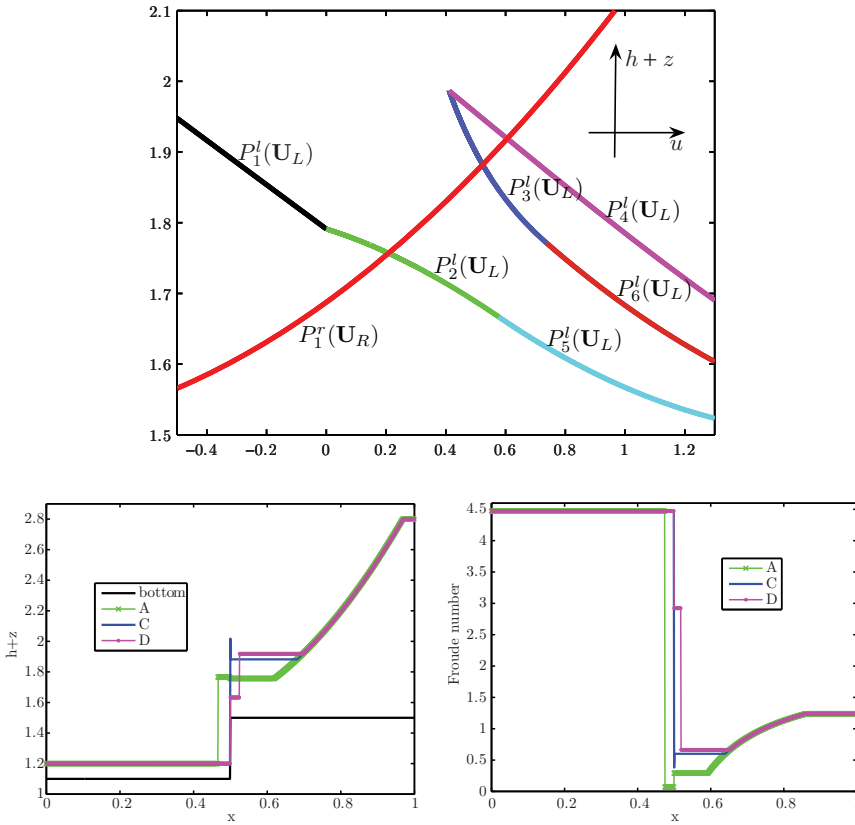
FIG. 31. Top: L–M curve $\bigcup\limits_{k=1}^{6} P_k^l(\mathbf{U}_L)$. Bottom left: The water free surface $h + z$ at $t = 1$. Bottom right: the Froude number. The Riemann initial data are given in (4.76).

We define

$$u_{0R}^* = u_c^* - 2c_c^*. \tag{4.86}$$

Note that if $h_L > 0$ and $u_{0L} > u_{0R}^*$, the curve $P_1^l(\mathbf{U}_L)$ and the R–M curve always have an intersection point. If the intersection point lies on $P_2^r(\mathbf{U}_R)$, the solution has the wave configuration A^T; see Figure 16. An example can be found in Figure 38. If the intersection point lies on $P_3^r(\mathbf{U}_R)$, the solution has the wave configuration F; see Figure 9. An example is shown in Figure 39. We can see that the resonant wave occurs around $x = 0.5$. Similarly, if the intersection point lies on $P_4^r(\mathbf{U}_R)$, the solution has the wave configuration G; see Figure 14. An example is shown in Figure 40.

However if $u_{0L} < u_{0R}^*$ and $h_L > 0$, the Riemann solution contains a dry bed state since there is no intersection point between $P_1^l(\mathbf{U}_L)$ and the R–M curve; see Figure 41. Specifically, the solution has the wave configuration G_v; see Figure 15. An example with $h_L > 0$ can be found in Figure 41. An example with $h_L < 0$ is shown in Figure 41. Here all of the examples are in the interval $[0, 1]$.
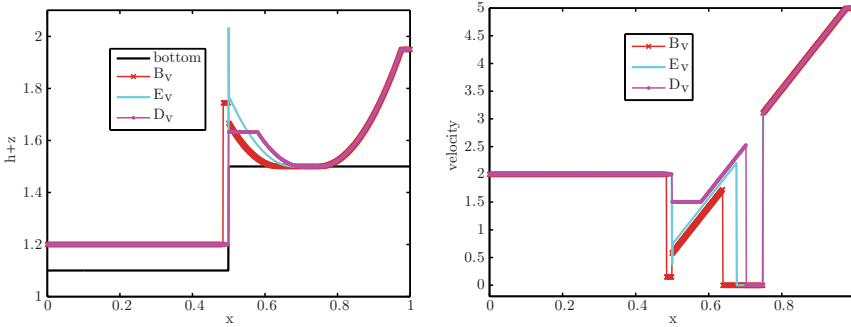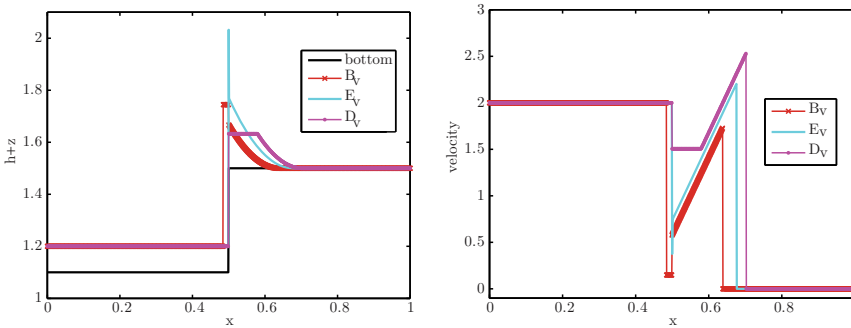
FIG. 32. Left: The water free surface $h + z$ at $t = 0.08$. Right: The
velocity. The Riemann initial data are $(z_L, h_L, u_L) = (1.1, 0.1, 2.0)$
when $x < 0.5$ and $(z_R, h_R, u_R) = (1.5, 0.45, 5.0)$ when $x > 0.5$.

FIG. 33. Left: The water free surface $h + z$ at $t = 0.08$. Right: The
velocity. The Riemann initial data are $(z_L, h_L, u_L) = (1.1, 0.1, 2.0)$
when $x < 0.5$ and $(z_R, h_R, u_R) = (1.5, 0, 0)$ when $x > 0.5$.

4.3.2. *CASE II_R*: $u_R + c_R < 0$. In this case the R–M curve also consists of four
segments, which are defined as follows:

$P_1^r(\mathbf{U}_R) = \{\mathbf{U} | \mathbf{U} \in T_2(\mathbf{U}_R) \text{ with } u > 0\}$,
$P_2^r(\mathbf{U}_R) = \{\mathbf{U} | \mathbf{U} = \mathbf{J}(z_L; \mathbf{U}_-, z_R) \text{ and } \mathbf{U}_- \in S_2^+(\mathbf{U}_L) \text{ with } \hat{u}_R < u_- < 0, \ \bar{\hat{u}}_R < u < 0\}$,
$P_3^r(\mathbf{U}_R) = \{\mathbf{U} | \mathbf{U} = \mathbf{J}(z_L; \mathbf{U}_+, z); \ \mathbf{U}_+ = S_2^0(\mathbf{U}_-); \ \mathbf{U}_- = \mathbf{J}(z; \mathbf{U}_R, z_R), z_L \leq z \leq z_R\}$,
$P_4^r(\mathbf{U}_R) = \{\mathbf{U} | \mathbf{U} \in T_2(\bar{\mathbf{U}}_R) \text{ with } u < \bar{\hat{u}}_R\}$,

where $\bar{\hat{\mathbf{U}}}_R = \mathbf{J}(z_L; \hat{\mathbf{U}}_R, z_R)$ and $\hat{\mathbf{U}}_R = S_2^0(\mathbf{U}_R)$, while $\bar{\hat{\mathbf{U}}}_R = S_2^0(\bar{\mathbf{U}}_R)$ and $\bar{\mathbf{U}}_R = \mathbf{J}(z_L; \mathbf{U}_R, z_R)$. Analogously to CASE I_R, the R–M curve in this case is continuous
and strictly increasing in the state space $(u, h + z)$.

We define
$$u_{0R}^* = \bar{u}_R - 2\bar{c}_R. \tag{4.87}$$
Note that if $u_{0L} > u_{0R}^*$ and $h_L > 0$, the curve $P_1^l(\mathbf{U}_L)$ and the R–M curve always
have an intersection point. If the intersection point lies on $P_2^r(\mathbf{U}_R)$, the solution has
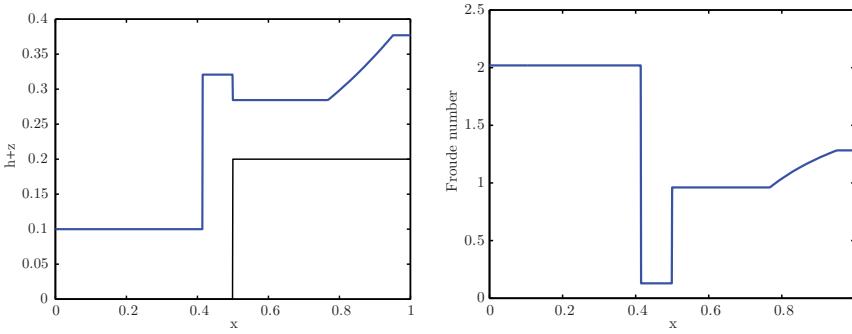the wave configuration A^T. This is the same as for the solution related to the segment

FIG. 34. Left: The water free surface $h + z$ at $t = 0.15$. Right: The Froude number. The Riemann initial data are $(z_L, h_L, u_L) = (0.0, 0.1, 2.0)$ when $x < 0.5$ and $(z_R, h_R, u_R) = (0.2, 0.177, 1.69)$ when $x > 0.5$.
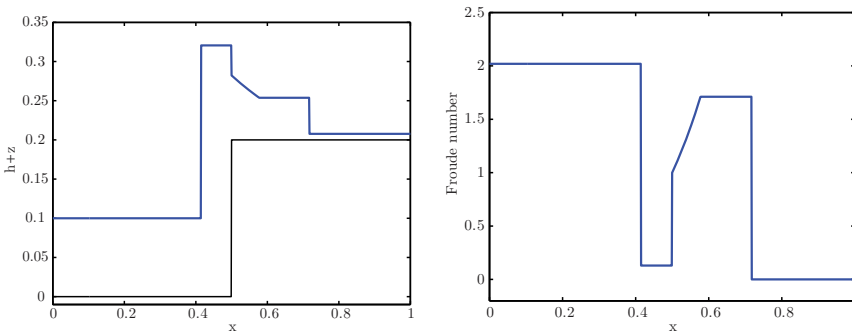

FIG. 35. Left: The water free surface $h + z$. Right: The Froude number at $t = 0.15$. The Riemann initial data are $(z_L, h_L, u_L) = (0.0, 0.1, 2.0)$ when $x < 0.5$ and $(z_R, h_R, u_R) = (0.2, 0.0077, 0.0)$ when $x > 0.5$.

$P_2^r(\mathbf{U}_R)$ in CASE I_R. If the intersection point lies on $P_3^r(\mathbf{U}_R)$, the solution has the wave configuration C^T; see Figure 17. An example is shown in Figure 43. We can see that the resonant wave occurs around $x = 0.5$. If the intersection point lies on $P_4^r(\mathbf{U}_R)$, the solution has the wave configuration D^T; see Figure 18. An example is shown in Figure 44.

Otherwise, if $u_{0L} < u_{0R}^*$ or $h_L > 0$, the solution has the wave configuration D_v^T. An example with $h_L > 0$ is shown in Figure 45. An example with $h_L = 0$ is shown in Figure 46.

5. Algorithm for exact Riemann solutions to the shallow water equations. In this section we present an algorithm for solving the exact Riemann problem for (1.1) and (1.3) under the assumption $z_L < z_R$. For the given Riemann initial data, if $h_L = h_R = 0$, the solution is $h = 0$ and $u = 0$ for $(x, t) \in \mathbb{R} \times \mathbb{R}^+$. So in the following we always assume that $h_L = 0$ and $h_R = 0$ cannot occur.
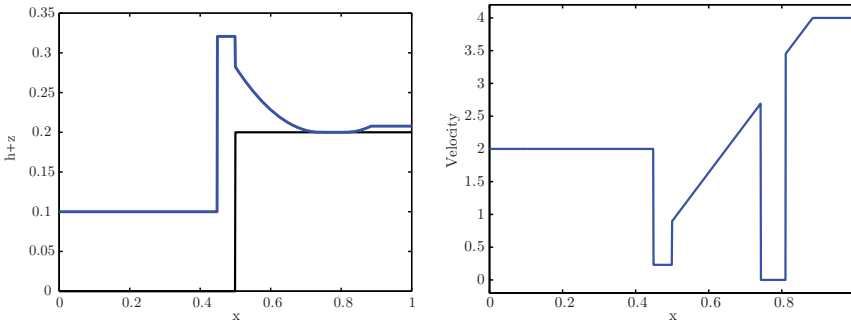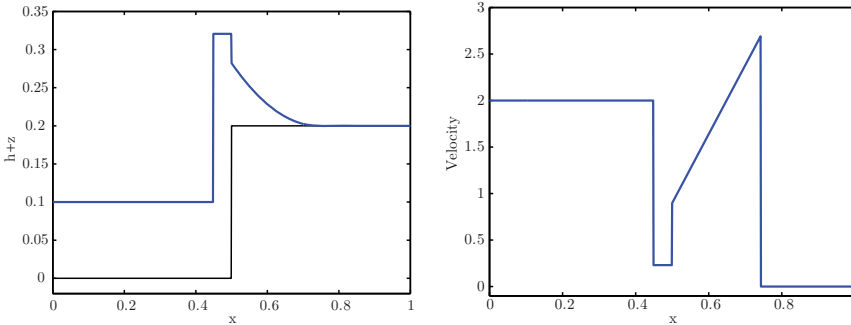
FIG. 36. Left: The water free surface $h + z$. Right: The Froude number at $t = 0.09$. The Riemann initial data are $(z_L, h_L, u_L) = (0.0, 0.1, 2.0)$ when $x < 0.5$ and $(z_R, h_R, u_R) = (0.2, 0.0077, 4.0)$ when $x > 0.5$.

FIG. 37. Left: The water free surface $h + z$. Right: The Froude-number at $t = 0.09$. The Riemann initial data are $(z_L, h_L, u_L) = (0.0, 0.1, 2.0)$ when $x < 0.5$ and $(z_R, h_R, u_R) = (0.2, 0, 0)$ when $x > 0.5$.

If $h_L = 0$, there is no L–M curve. Otherwise, if $h_L > 0$ but $u_{0L} < 0$, the L–M curve contains only one segment which is $P_1^l(\mathbf{U}_L)$, defined in (4.3). Analogous to the R–M curves, if $h_R = 0$, there is no R–M curve. Otherwise, if $h_R > 0$ but $u_{0R} > 0$, the R–M curve contains only one segment which is $P_1^r(\mathbf{U}_R)$, defined in (4.5). The common point of these cases is that there is no stationary wave on the L–M and R–M curves. Generally there are three types of possible solutions:

(1) If $h_L = 0$ and $u_{0R} > 0$, the solution is defined in (2.27);
(2) If $h_R = 0$ and $u_{0L} < 0$, the solution is defined in (2.25);
(3) If $u_{0L} < 0$ and $u_{0R} > 0$, the solution has the wave configuration A_v.

Besides, if $u_{0L} > 0$ or $u_{0R} < 0$, the stationary wave exists except in the case when $h_L^{max} + z_L < h_R^{max} + z_R$ and $u_{0R} > 0$. Note that if $u_{0R} > 0$, we have $h_R^{max} = 0$. Therefore by (4.14) we obtain $z_{max} < z_R$, i.e. CASE I_L occurs.
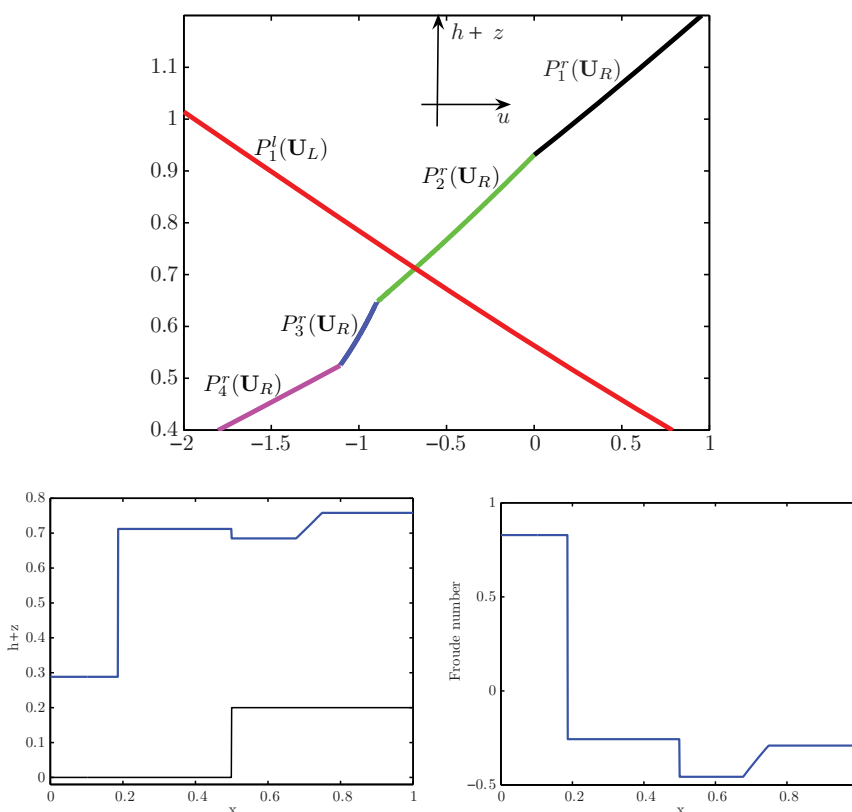
FIG. 38. Top: R–M curve $\bigcup_{k=1}^{4} P_k^r(\mathbf{U}_R)$. Bottom left: The water free surface $h + z$ at $t = 0.15$. Bottom right: The Froude number. The Riemann initial data are $(z_L, h_L, u_L) = (0.0, 0.2883, 1.393)$ when $x < 0.5$ and $(z_R, h_R, u_R) = (0.2, 0.558, -0.68)$ when $x > 0.5$.

Consider the case when the stationary wave exists. If $h_L^{max} + z_L < h_R^{max} + z_R$ and $u_{0R} < 0$, we have $u_M < 0$. Hence the stationary wave is on the R–M curve. Otherwise the stationary wave is on the L–M curve.

According to our construction, the L–M curve is classified into 5 different cases, while the R–M curve is classified into 2 different cases. Every case contains different types of wave configurations. Each type of wave configuration corresponds to a specific segment of the wave curve. The intermediate state (h_M, u_M) of the exact Riemann solution is the intersection point of segments of the L–M and R–M curves. The L–M curve, in the absence of CASES III_L and IV_L involving the bifurcation, is strictly decreasing while the R–M curve is strictly increasing in the $(u, h + z)$ state space. This monotonicity behavior of the curves guarantees that the intersection point exists uniquely. Moreover, the L–M curve in CASES III_L and IV_L consists of more than one branch.
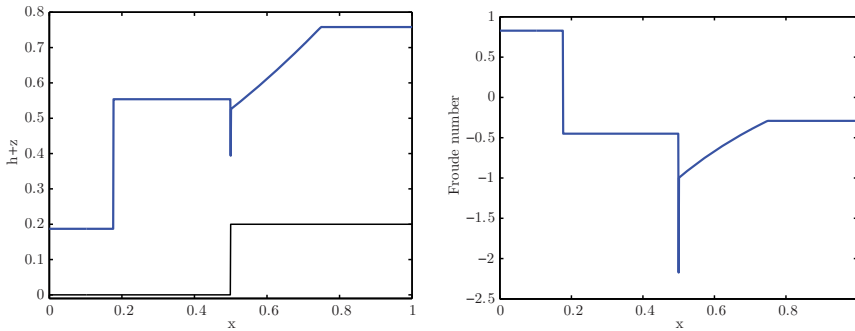
FIG. 39. Left: The water free surface $h + z$ at $t = 0.15$. Right: The Froude number. The Riemann initial data are $(z_L, h_L, u_L) = (0.0, 0.1871, 1.1222)$ when $x < 0.5$ and $(z_R, h_R, u_R) = (0.2, 0.558, -0.68)$ when $x > 0.5$.
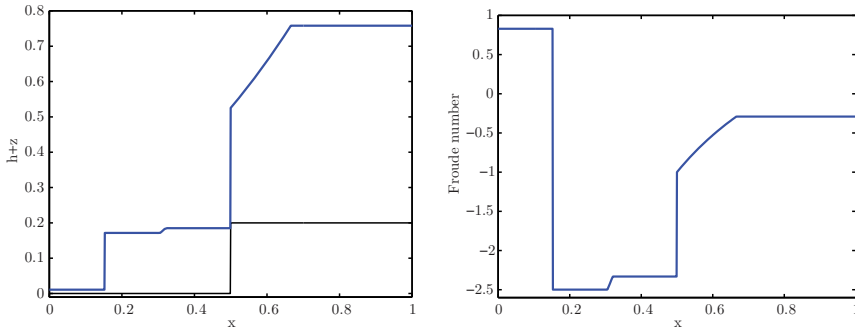

FIG. 40. Left: The water free surface $h + z$ at $t = 0.1$. Right: The Froude number. The Riemann initial data are $(z_L, h_L, u_L) = (0.0, 0.0109, 0.2712)$ when $x < 0.5$ and $(z_R, h_R, u_R) = (0.2, 0.558, -0.68)$ when $x > 0.5$.

Every branch, however, is strictly decreasing. So every solution exists uniquely on the corresponding branch.

We present the algorithm for the exact Riemann solutions of (1.1) and (1.3) with $z_L < z_R$ in Algorithm 4. Because of space limitations we just take the modular unit CASE III_L as an example to show the algorithm for the L–M and R–M curves. Note that the L–M curve in CASE III_L contains bifurcation. Also the solver for the wave configuration A, see Algorithm 3, is presented as an example to calculate the intermediate state (u_M, h_M). The remaining cases of L–M and R–M curves and wave configurations can be dealt with in similar ways. The bisection method is used to solve the nonlinear system. Of course we can also adopt other iteration methods, say the secant method, to solve the problem. The Newton method is not so easy to apply because it is complicated to compute the derivative of the corresponding function.
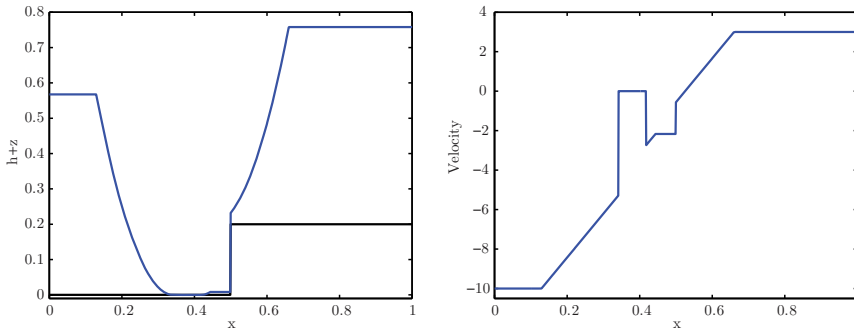
FIG. 41. Left: The water free surface $h + z$ at $t = 0.03$. Right: The Froude number. The Riemann initial data are $(z_L, h_L, u_L) = (0.0, 0.5674, -10)$ when $x < 0.5$ and $(z_R, h_R, u_R) = (0.2, 0.558, 3.0)$ when $x > 0.5$.
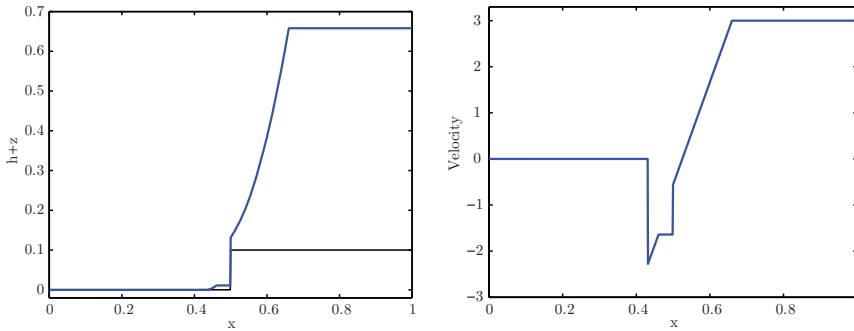

FIG. 42. Left: The water free surface $h + z$ at $t = 0.03$. Right: The Froude number. The Riemann initial data are $(z_L, h_L, u_L) = (0, 0, 0)$ when $x < 0.5$ and $(z_R, h_R, u_R) = (0.1, 0.558, 3.0)$ when $x > 0.5$.

6. Conclusion. For any given Riemann initial data $\mathbf{U}_L$ and $\mathbf{U}_R$ with $z_L < z_R$, we obtain all possible Riemann solutions to the shallow water equation by constructing the L–M and R–M curves. We analyze the behavior of the L–M and R–M curves. We observe that on one hand if the intersection points belong to CASES III_L and IV_L of the L–M curves, a bifurcation appears on the L–M curves. There may be three possible solutions due to the bifurcation. In the other cases, the solution always uniquely exists. The dry bed problem has also been considered in this framework. Here the dry bed problem refers to two subcases. One is for the water propagating to a dry bed, i.e. $h_L = 0$ or $h_R = 0$. The other one is for the dry bed state emerging due to the motion of the flow.
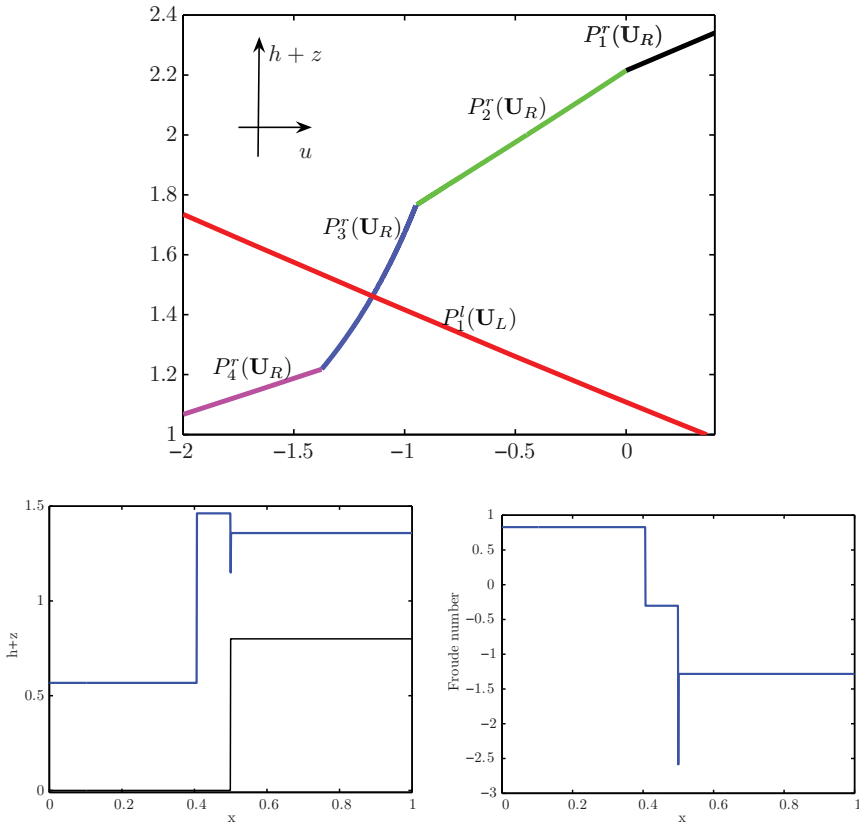
FIG. 43. Top: R–M curve $\bigcup\limits_{k=1}^{4} P_k^r(\mathbf{U}_R)$. Bottom left: The water free surface $h + z$. Bottom right: The Froude number at $t = 0.03$. The Riemann initial data are $(z_L, h_L, u_L) = (0.0, 0.5674, 1.9542)$ when $x < 0.5$ and $(z_R, h_R, u_R) = (0.8, 0.558, -3.0)$ when $x > 0.5$.
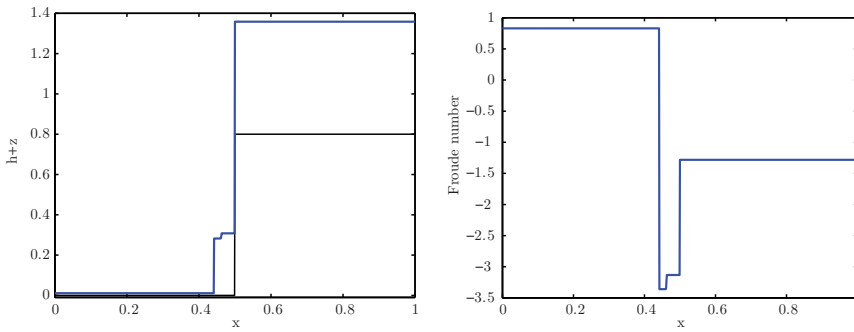
FIG. 44. Left: The water free surface $h + z$. Right: The Froude number at $t = 0.01$. The Riemann initial data are $(z_L, h_L, u_L) = (0.0, 0.0109, 0.2712)$ when $x < 0.5$ and $(z_R, h_R, u_R) = (0.8, 0.558, -3.0)$ when $x > 0.5$.

FIG. 45. Left: The water free surface $h + z$ at $t = 0.025$. Right: The Froude number. The Riemann initial data are $(z_L, h_L, u_L) = (0.0, 0.5574, -14.0)$ when $x < 0.5$ and $(z_R, h_R, u_R) = (0.1, 0.558, -3.0)$ when $x > 0.5$.
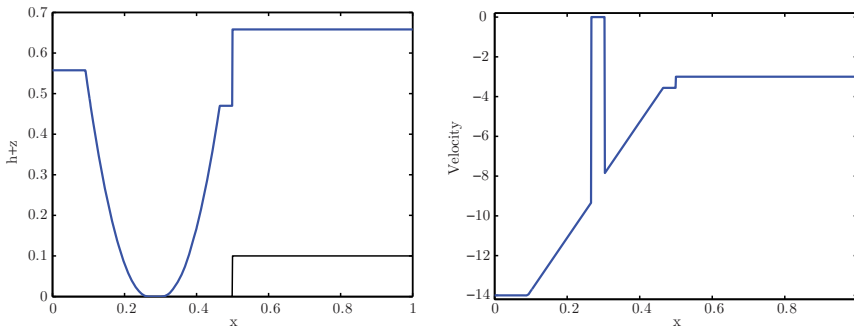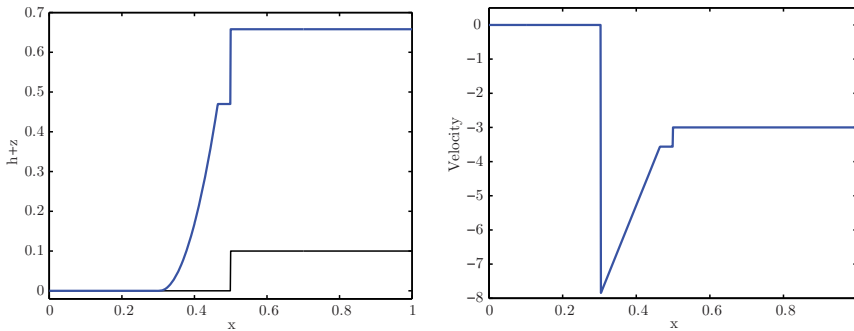

FIG. 46. Left: The water free surface $h + z$ at $t = 0.025$. Right: The Froude number. The Riemann initial data are $(z_L, h_L, u_L) = (0, 0, 0)$ when $x < 0.5$ and $(z_R, h_R, u_R) = (0.1, 0.558, -3.0)$ when $x > 0.5$.

Algorithm 2 Modular unit for CASE III_L

Require: $u_{0L} > u_{0R}$, $u_L > c_L$, $z_R < z_S$
1: $u_{0L}^* \leftarrow \bar{u}_L + 2\bar{c}_L$
2: **if** $u_{0L}^* > u_{0R}$ **then**
3:     $u_1 \leftarrow u_R + f(\bar{\hat{u}}; h_R)$, $u_2 \leftarrow u_R + f(\hat{\hat{u}}; h_R)$
4:     **if** $u_2 < \hat{\bar{u}}_L$ **then**
5:         Solver for the wave configuration A in Algorithm 3
6:     **else if** $u_1 < \bar{\hat{u}}_L$ **then**
7:         Solver for the wave configuration A in Algorithm 3
8:         Solver for the wave configuration C
9:         Solver for the wave configuration D
10:     **else**
11:         Solver for the wave configuration D
12:     **end if**
13: **else**
14:     Sample for the wave configuration D_v
15: **end if**

Algorithm 3 Solver for the wave configuration A

Require: h_l, h_r and ϵ

1: $u_l \leftarrow u_L - f(h_l; h_L)$, $u_r \leftarrow u_L - f(h_r; h_L)$
2: $\bar{\mathbf{U}}_l \leftarrow J(z_R; \mathbf{U}_l, z_L)$, $\bar{\mathbf{U}}_r \leftarrow J(z_R; \mathbf{U}_r, z_L)$.
3: $f_1 \leftarrow \bar{u}_l - u_R - f(\bar{h}_l; h_R)$, $f_2 \leftarrow \bar{u}_r - u_R - f(\bar{h}_r; h_R)$.

Require: $f_1 \dot{f}_2 < 0$

4: **if** $\|f_1\| < \epsilon$ **then**
5:     **return** $(\bar{u}_l, \bar{h}_l)$
6: **else if** $\|f_2\| < \epsilon$ **then**
7:     **return** $(\bar{u}_r, \bar{h}_r)$
8: **else**
9:     $h_{mid} \leftarrow \frac{h_l + h_r}{2}$, $u_{mid} \leftarrow u_L - f(h_{mid}; h_L)$
10:     $\bar{\mathbf{U}}_{mid} \leftarrow J(z_R; \mathbf{U}_{mid}, z_L)$
11:     $f_{mid} \leftarrow \bar{u}_{mid} - u_R - f(\bar{h}_{mid}; h_R)$
12:     **while** $\|f_{mid}\| > \epsilon$ **do**
13:         **if** $f_{mid} \cdot f_1 > 0$ **then**
14:             $h_l \leftarrow h_{mid}$
15:         **else**
16:             $h_r \leftarrow h_{mid}$
17:         **end if**
18:         go to 9,10 and 11
19:     **end while**
20: **end if**

Algorithm 4 Algorithm for the exact Riemann solutions

Require: $\mathbf{U}_L$, $\mathbf{U}_R$, $z_L < z_R$

1:   $u_{0L} \leftarrow u_L + 2c_L$, $u_{0R} \leftarrow u_R - 2c_R$
2:   **if** $u_{0L} < 0 \wedge h_R = 0$ **then**
3:      Sample solution in (2.25)
4:   **else if** $u_{0R} > 0 \wedge h_L = 0$ **then**
5:      Sample solution in (2.27)
6:   **else if** $u_{0R} > 0 \wedge u_{0L} < 0$ **then**
7:      Sample solution in the wave configuration A_v
8:   **else**
9:      calculate h_L^{max} by (4.13) and $z_{max} \leftarrow z_L + h_L^{max}$
10:     **if** $z_{max} < h_R^{max} + u_{0R}$ and $u_{0R} > 0$ **then**
11:       **if** $u_R + c_R \geq 0$ **then**
12:         Modular unit for CASE I_R
13:       **else**
14:         Modular unit for CASE II_L
15:       **end if**
16:     **else**
17:       **if** $z_{max} < z_R$ **then**
18:         **if** $h_R = 0$ **then**
19:           sample the solution in the wave configuration H_2
20:         **else if** $u_{0R} > 0$ **then**
21:           sample the solution in the wave configuration H_2
22:         **end if**
23:       **else if** $u_L < c_L$ **then**
24:         Modular unit for CASE II_L
25:       **else if** $u_L > c_L$ **then**
26:         calculate z_T by (4.21) and z_S by (4.16)
27:         **if** $z_R < z_S$ **then**
28:           Modular unit for CASE III_L in Algorithm 2
29:         **else if** $z_R < z_T$ **then**
30:           Modular unit for CASE IV_L
31:         **else**
32:           Modular unit for CASE V_L
33:         **end if**
34:       **end if**
35:     **end if**
36:   **end if**

References

[1] Ashwin Chinnayya, Alain-Yves LeRoux, and Nicolas Seguin, *A well-balanced numerical scheme for the approximation of the shallow-water equations with topography: The resonance phenomenon*, Int. J. Finite Vol. **1** (2004), no. 1, 33. MR2465450 (2009j:65186)

[2] J.J. Stoker, *Water Waves*, Interscience,. New York, 1957.

[3] Nikolai Andrianov, *Performance of numerical methods on the non-unique solution to the Riemann problem for the shallow water equations*, Internat. J. Numer. Methods Fluids **47** (2005), no. 8-9, 825–831, DOI 10.1002/fld.846. MR2123795 (2005i:76079)

[4] Nikolai Andrianov and Gerald Warnecke, *The Riemann problem for the Baer-Nunziato two-phase flow model*, J. Comput. Phys. **195** (2004), no. 2, 434–464, DOI 10.1016/j.jcp.2003.10.006. MR2046106 (2004m:76165)

[5] Francisco Alcrudo and Fayssal Benkhaldoun, *Exact solutions to the Riemann problem of the shallow water equations with a bottom step*, Comput. & Fluids **30** (2001), no. 6, 643–671, DOI 10.1016/S0045-7930(01)00013-5. MR1859269 (2002g:76012)

[6] F. Benkhaldoun and L. Quivy, *A Non Homogeneous Riemann Solver for shallow water and two phase flows*, Flow, Turbulence and Combustion **76** (2006), pp. 391-402.

[7] R. Bernetti, V. A. Titarev, and E. F. Toro, *Exact solution of the Riemann problem for the shallow water equations with discontinuous bottom geometry*, J. Comput. Phys. **227** (2008), no. 6, 3212–3243, DOI 10.1016/j.jcp.2007.11.033. MR2392731 (2009a:76015)

[8] R. W. D. Nickalls, *A New Approach to Solving the Cubic: Cardan's Solution Revealed*, The Mathematical Gazette, **77** (Nov., 1993), pp. 354-359.

[9] E. Han, M. Hantke, and G. Warnecke, *Exact Riemann solutions in ducts with discontinuous cross–section*, J. Hyp. Diff. Equations **9** (2012), pp. 403-449.

[10] Jiequan Li and Guoxian Chen, *The generalized Riemann problem method for the shallow water equations with bottom topography*, Internat. J. Numer. Methods Engrg. **65** (2006), no. 6, 834–862, DOI 10.1002/nme.1471. MR2200026 (2006j:76022)

[11] E. F. Toro, *The Dry–Bed Problem in Shallow–Water Flows*, College of Aeronautics Reports, 1990.

[12] E. F. Toro, *Shock-Capturing Methods for Free-Surface Shallow Flows*, Wiley and Sons. Ltd., 2001.

[13] Eli Isaacson and Blake Temple, *Nonlinear resonance in systems of conservation laws*, SIAM J. Appl. Math. **52** (1992), no. 5, 1260–1278, DOI 10.1137/0152073. MR1182123 (93f:35140)

[14] Jihwan Kim and Randall J. LeVeque, *Two-layer shallow water system and its applications*, Hyperbolic problems: Theory, numerics and applications, Proc. Sympos. Appl. Math., vol. 67, Amer. Math. Soc., Providence, RI, 2009, pp. 737–743. MR2605269 (2011e:76024)

[15] Paola Goatin and Philippe G. LeFloch, *The Riemann problem for a class of resonant hyperbolic systems of balance laws* (English, with English and French summaries), Ann. Inst. H. Poincaré Anal. Non Linéaire **21** (2004), no. 6, 881–902, DOI 10.1016/j.anihpc.2004.02.002. MR2097035 (2006i:35225)

[16] V. V. Ostapenko, *Dam-break flows over a bottom step* (Russian, with Russian summary), Prikl. Mekh. Tekhn. Fiz. **44** (2003), no. 4, 51–63, DOI 10.1023/A:1024292822989; English transl., J. Appl. Mech. Tech. Phys. **44** (2003), no. 4, 495–505. MR2009465 (2004e:76026)

[17] D. Rochette, S. Clain, and W. Bussière, *Unsteady compressible flow in ducts with varying cross–section: Comparison between the nonconservative Euler system and axisymmetric flow model. Preprint submitted.

[18] Philippe G. LeFloch, *Kinetic relations for undercompressive shock waves. Physical, mathematical, and numerical issues*, Nonlinear partial differential equations and hyperbolic wave phenomena, Contemp. Math., vol. 526, Amer. Math. Soc., Providence, RI, 2010, pp. 237–272, DOI 10.1090/conm/526/10384. MR2731995 (2012d:35222)

[19] Philippe G. LeFloch and Mai Duc Thanh, *The Riemann problem for the shallow water equations with discontinuous topography*, Commun. Math. Sci. **5** (2007), no. 4, 865–885. MR2375051 (2009k:35179)

[20] Philippe G. LeFloch and Mai Duc Thanh, *A Godunov-type method for the shallow water equations with discontinuous topography in the resonant regime*, J. Comput. Phys. **230** (2011), no. 20, 7631–7660, DOI 10.1016/j.jcp.2011.06.017. MR2823568 (2012g:76028)

[21] D. Marchesin and P. J. Paes-Leme, *A Riemann problem in gas dynamics with bifurcation*: Hyperbolic partial differential equations, III, Comput. Math. Appl. Part A **12** (1986), no. 4-5, 433–455. MR841979 (87e:76106)